



UNIVERSITÀ DEGLI STUDI DI PADOVA

Dipartimento di Fisica e Astronomia “Galileo Galilei”

Master Degree in Physics

Final Dissertation

Mode controllability of a Network Random Laser

Thesis supervisor

Prof. Giovanni Mattei

Thesis co-supervisor

Dr. Riccardo Sapienza

Candidate

Oscar Cipolato

Academic Year 2019/2020

UNIVERSITÀ DEGLI STUDI DI PADOVA

Dipartimento di Fisica e Astronomia "Galileo Galilei"

Abstract

Mode controllability of a Network Random Laser

by Oscar CIPOLATO

Nanophotonic networks, micrometer-scale systems made of interconnected sub-wavelength waveguides, have important applications in quantum optics and integrated photonics. Random lasing is often uncontrolled in emission wavelength, directions and temporal dynamics. The complexity of the photonic network lasers allows the formation of spatially localized E.M. modes and brings the opportunity to control the lasing action by selectively illuminating a small subset of the network links. This result is predicted by a graph description of Maxwell's equations, which is used to model the network laser. A computational procedure that can be experimentally implemented to select a single mode is developed and its results studied. The experimental mode selection procedure is tested on a sample using adaptive pumping, achieving mode controlling.

Acknowledgements

I want to thank all the people who helped me along this long journey. First of all I'd like to thank Dr. Riccardo Sapienza: he has been a wonderful project supervisor and mentor. I must also thank Riccardo's research group members for their kindness and positive attitude, in particular Dr. Dhruv Saxena, that helped me throughout the whole research project. I want to thank Prof. Giovanni Mattei for his useful advice and his willingness to help me in various situations. I must also be grateful to all my friends and colleagues: thanks to Andrea Ludovici for those long days of studying and debating; thanks to my former lab group members Dimitri Tavian, Luigi Angelini, Luca Zago and Gianmarco Puggioni; thanks to Matteo Polo and Martino Calzavara for all the pleasurable time spent together; thanks to all the people that lent me their notes, revised with me, and gave me useful advice (and that's a lot of people). My thanks to my wonderful ICL flatmates and Erasmus friends for all the good times I had with you. Lastly, I need to thank those people who make "Borse di Studio Regionali" available to many needy students every year.

Contents

Acknowledgements	v
1 Introduction	1
2 Lasers: conventional VS random	3
2.1 Conventional Laser	3
2.2 Random Laser	5
3 The network approach to photonics	9
3.1 Network theory	9
3.2 Network Random Laser	11
3.2.1 Calculating the modes of a NRL	12
4 Numerical simulations of NRL	15
4.1 Mode selection code	15
4.2 Results of the numerical simulations	16
4.3 Discussion of modeling results	23
5 Experimental part	25
5.1 Methods employed in the experiment part	25
5.1.1 The experimental NRL sample	25
5.1.2 Experimental setup	26
5.1.3 Experimental mode selection routine	29
5.1.4 Experimental procedure	30
5.2 Results in the experimental part	31
5.2.1 Lasing behaviour check and preliminary measurements	31
5.2.2 Evidence of non-linear behaviour	36
5.2.3 Issues with spectrum outputs	39
5.2.4 Mode controlling	42
6 Concluding chapter	55
6.1 Future developments	55
6.2 Conclusions	55

Chapter 1

Introduction

Network science describes complex systems looking at the interaction between the elementary units, neglecting microscopic details. The network approach has been successfully used in a plethora of topics in different disciplines [1]: to understand the way a virus spreads, quantum information is transmitted, or a power grid failure propagates. Likewise in nanophotonics, a network approach can be useful to understand emission, scattering, and concentration of light in complex photonic systems [2, 3].

A particular field of research in nanophotonics where the network approach can be useful is random lasing. A random laser is a device where the optical feedback is provided by scattering mechanisms or randomly placed elements instead of reflecting components. Such systems usually are more difficult to control and their properties more difficult to predict, but show some unique and interesting features. Network Random Lasers (NRL) is a type of random laser that can be easily modeled and studied using the network approach.

An experimental realization of such laser has already been built and demonstrated [4]. However, many of the interesting properties of this system, such as the mode controllability, that may be useful for future applications, still need to be understood completely. Therefore, the aim of this project is to design and test a reliable procedure to control the lasing properties of a network random laser, in order to study and understand the mode controllability of such system. This task will be addressed both computationally and experimentally.

In this thesis the lasing from network random laser is studied, focusing on the possibility of controlling the spectrum of the laser changing the pumping profile in order to achieve a single-mode laser device. This is addressed both computationally with a MATLAB and Python code, and experimentally on a dye-doped polymer fibre mesh.

This thesis is structured as follows:

In **chapter 2** the random lasers are introduced, their differences with conventional lasers and their features are explained.

In **chapter 3** the network approach to random lasers is explained and Network Random Laser is introduced.

In **chapter 4** the modeling part is explained: the network approach to lasing in the NRL is described in detail and the code for mode selection is presented; the mode selection results are shown for a Buffon-type network; the results of the mode selection code are explained and discussed, putting particular

emphasis on the key optimization parameters and control parameters.

In **chapter 5** the experimental part is presented: the experimental apparatus, and experimental procedure are described and motivated; the lasing activity is checked in two different samples and the mode selection procedure is run on the samples; comments about the lasing in samples are presented and the results of the mode selection procedure are discussed.

In **chapter 6** possible future developments are explained and the outline of this work is recapitulated.

Chapter 2

Lasers: conventional VS random

In this chapter an introduction about lasers is given, with a focus on the main parts that are necessary in a laser device and how these affect its behaviour. Random lasing will be introduced with a brief historical overview and its differences with conventional laser devices will be clearly pointed out.

2.1 Conventional Laser

A laser is a device that emits light amplified by stimulated emission (*LASER* = Light Amplification by Stimulated Emission of Radiation) [5]. A laser differs from other sources of light in that it emits light coherently. Spatial coherence allows a laser to be focused to a tight spot and to stay narrow over great distances (collimation). Lasers can also have high temporal coherence, which allows them to emit light with a very narrow spectrum.

Stimulated emission is one of three processes that can happen between two quantum energy levels (atomic electron levels or molecular excited states), the other two being *spontaneous emission* and *absorption* (see figure 2.1). Given two levels of energy E_1 and E_2 , such that $E_2 - E_1 = \Delta E > 0$, these are the features of these three processes:

- Spontaneous emission: an excited state can spontaneously decay into a lower energy level after some time, releasing energy in the form of a photon, emitted in a random spatial direction. The frequency of the photon ν is given by the equation $\Delta E = h\nu$, where h is Planck constant.
- Absorption: an incoming photon of frequency $\nu = \Delta E/h$ can be absorbed by the lower energy state, causing the transition to the higher energy level.
- Stimulated emission: an incoming photon of frequency $\nu = \Delta E/h$ can interact with the excited state, causing it to drop to a lower energy level. The energy is released in the form of a photon, with a phase, frequency, polarization, and direction of travel that are all identical to the photons of the incident wave. This last feature is responsible for the characteristic properties of lasers.

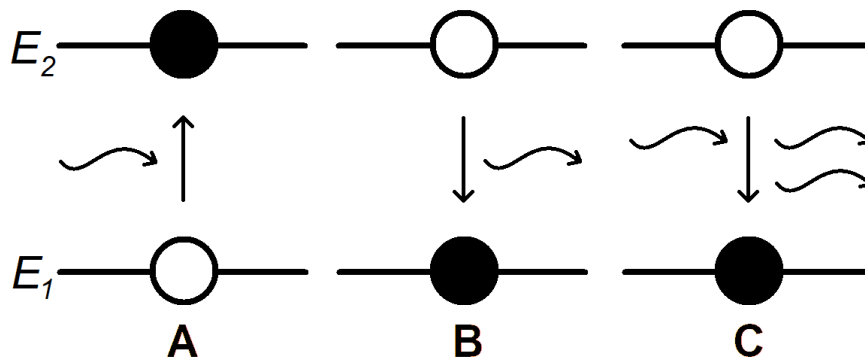


FIGURE 2.1: The three processes that can happen between two quantum energy levels (E_1 and E_2): A) Absorption; B) Spontaneous emission; C) Stimulated emission.

In order to achieve lasing the number of species in the excited state N_2 must be higher than the number of species in the lower state N_1 . This configuration is called *population inversion*. This is only possible if the system is externally pumped and if the system has an appropriate energy structure.

There are three principal parts in any laser (see figure 2.2): gain medium, optical resonator and pump source. These are their functions:

- **Optical resonator:** an arrangement of optical components which allows a beam of light to circulate in a closed path, in which the gain medium is placed. Such resonators can be made in very different forms (*e.g.* mirrors or waveguides in conventional lasers). They are usually necessary since, in most cases, multiple passes through the medium are required to achieve enough gain. Its features define the *resonator modes* (*i.e.* electric field distributions that are self-reproducing in each resonator round trip, apart from a possible loss of power), therefore the wavelengths of the laser and its directionalities.
- **Gain medium (or active laser medium):** a medium that can exhibit population inversion and provide gain, used to amplify the power of light. Some examples are doped crystals, gases, and laser dyes. It defines the possible wavelengths of the laser. Since the gain medium cannot provide infinite gain, spatially overlapping modes will compete for the gain of the medium: this effect is called *mode competition*.
- **Pump source:** provides the gain medium with the energy required to produce excited states, necessary to achieve population inversion and sustain lasing. The pump energy is usually provided optically or electrically.

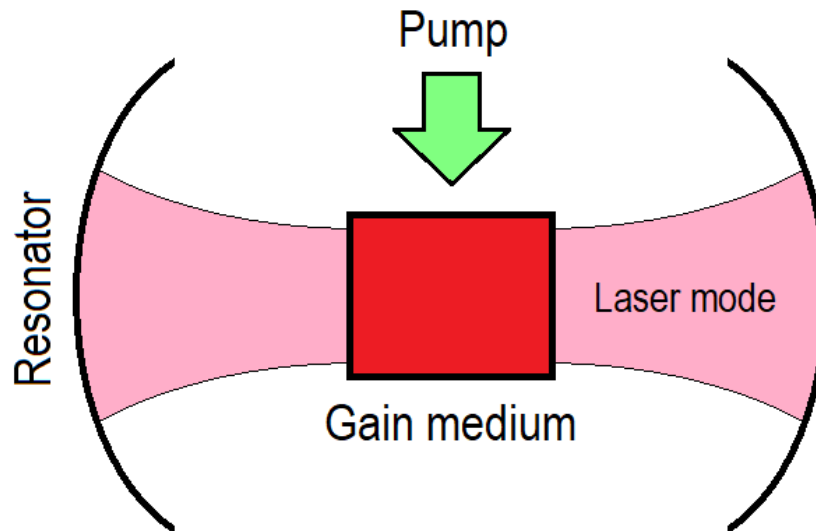


FIGURE 2.2: Scheme of a conventional laser. The three principal parts can be identified: gain medium; optical resonator; pump source. The optical resonator defines the laser modes (electric field distributions that are self-reproducing in each resonator round trip).

The choice of gain medium and optical resonator define the type and features of the laser.

2.2 Random Laser

A *Random Laser* (RL) is a laser in which optical feedback is provided by scattering particles: the optical resonator is composed by neither reflective surfaces nor distributed periodic structures (used in conventional lasers), as light is confined in the active region by diffusive elements interacting between themselves. In a random laser the multiple scattering process defines optical modes with a certain central frequency and bandwidth, lifetime and spatial profile. Therefore, random lasers are “mirror-less” but not “mode-less”, in contrast to amplified spontaneous emission, that is often classified as lasing without mirrors.

Multiple scattering due to randomness is intrinsically present in natural materials as well as photonic materials, such as photonic crystals, used in optical devices. Disorder in photonic materials is an unwanted property that is difficult to avoid and forms a major industrial bottleneck. However, multiple scattering can be exploited to introduce new functionalities.

This concept was first proposed by V. S. Letokhov in 1968 [6]: in his work, Letokhov considers a system where, instead of having a Fabri-Pérot resonator that confines light and allows it to travel multiple times in the active medium, the confinement is removed and some scattering elements are introduced in the active medium. Letokhov demonstrates theoretically that lasing action is possible even without confinement since the scattered light resides in the

active medium for much longer than it would without scattering elements; the system exhibits many modes that are strongly coupled by scattering and have large radiation losses. This theoretical work was first demonstrated experimentally by Lawandy and Balachandran in 1996 [7]: firstly, a rhodamine 640 dye in methanol solutions was used and the resulting spectrum acquired; then the same solution with the addition of 250 nm TiO₂ (rutile nanoparticles) was used and the resulting spectrum acquired. While the spectrum for the solution without scattering particles is compatible with a fluorescent spectrum, the spectrum of the solution with scattering particles displays a narrow peak that is 100 times more intense than the signal received in the previous spectra, thus demonstrating lasing action in the presence of scattering particles in an active medium.

The systems that were proposed did not take into account the fact that light could scatter around the sample and eventually bounce back into its own path, since it was expected to be very unlikely: until now no wave interference effect was mentioned, therefore only incoherent and non-resonant lasing was taken into account. Indeed, the lasing peak found by Lawandy and Balachandran was not so narrow and resolved as usual laser peaks. The type of feedback that we want to focus on now is field feedback, that is phase dependent and frequency dependent, in contrast to the previous intensity feedback. The only way to have coherent lasing is to take into account the wave nature of light and interference effects, considering the formation of closed paths and coherent feedback. As a consequence, a higher degree of scattering elements are needed to see this effect experimentally. Coherent random lasing was firstly demonstrate by H. Cao *et al.* in 1999 [8] and by S. V. Florov in the same year [9]. Cao report the first observation of random laser action with coherent feedback in semiconductor powder. In the experiment discrete lasing modes have been observed above the threshold, with laser emission from the powder observed in all directions. In Florov's experiment a dye-infiltrated opal photonic crystals was used. A stimulated emission regime, characterized by highly efficient, directional laser-like emission and a complex finely structured spectrum was found. In figure 2.3 a representation of incoherent and coherent random lasing is given.

The main theoretical issue with random lasers consists in the ability of the modes to collect enough gain from the material and start lasing, given the high losses of the system. During the last few years many articles and approaches to explain this issue have been produced. Many explanations of this phenomenon have been proposed, but it is likely that in each random lasers just few of these explanations are responsible for lasing action in that particular system. In 2004 Mujumdar [10] showed that the emission spikes are attributed to amplification of spontaneous emission along very long trajectories, because they are distinct from shot to shot and thus intrinsically stochastic. Therefore such behaviour is mainly due to the very rare photons with very long trajectories. In 2004 Apalkov *et al.* [11] showed that random lasing activity can be associated with pre-localized modes in the medium. In 2010 Ge *et al.* [12] suggested that random lasing is possible thanks to the presence of delocalized interacting modes. In random lasers with very high

degree of complexity the main responsible for lasing is Anderson localization, as proposed by Jiang and Soukoulis in 2000 [13] and Vanneste and Sebbah in 2001 [14]. This effect is known as *light localization*, the optical counterpart of Anderson localization of electrons [15]. The average spatial extent of these localized modes is called localization length. Only optical materials that are extremely scattering can support confined modes [16]. The Ioffe-Regel criterion expresses the requirement for light localization: the mean free path l needs to be smaller than the reciprocal wavevector, that is $kl \leq 1$.

In RLs modes are much more difficult to calculate and predict compared to conventional lasers, since the optical resonator is not formed by reflective surfaces or periodic structures, but an intrinsically disordered structure. The intensity of the modes is usually spread throughout the sample, making them extended modes. However, in some random materials, multiple scattering and interference can form randomly shaped but closed modes: confined modes with an exponential decay in amplitude.

Many random laser realizations have been created and studied: paint, powders and scattering particles in dye solution are few examples [17, 18, 19]. A particularly interesting feature of RLs that arises from the non-linear behaviour of mode competition (present when different modes overlap spatially) is *mode controllability*: the possibility to control the mode of the laser (wavelength or directionality). This has been demonstrated in optofluidic random lasers [20] and microdisk lasers [21] by changing the optical pumping profile. Such feature could be useful in future applications, such as on-chip lasers and sensitive bio-sensors.

To summarize, some of the properties that make RLs interesting and possible applications [22] are:

- They can be created with simple technologies and at low cost. Powders, scattering particles suspended in a solution with laser dye or microspheres of active material are few examples. No expensive, high-precision and time-consuming procedures for laser fabrication are usually required for random lasers.
- Angular distribution of the output can be very broad, over the complete solid angle of 4π for 3-dimensional systems, or over 2π for 2-dimensional systems. This feature can be used by a multifunctional on-chip laser.
- Complex and sensitive emission spectrum. The complexity can be used for document encoding; the sensitivity can be exploited for optical bio-sensing.
- They can be prepared in the form of suspension of particles that can be applied as coating on surfaces of arbitrary shape.

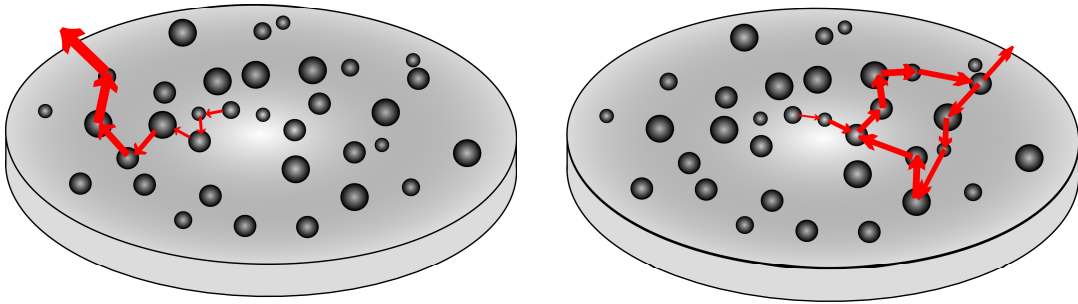


FIGURE 2.3: Representation of incoherent (left) and coherent (right) random lasing. While in incoherent random lasing light does not interfere with itself, in coherent lasing some closed paths form and interference effects become important.

Chapter 3

The network approach to photonics

In this chapter network theory is introduced and its relevance for photonic complex systems explained. The concept of Network Random Laser is presented and a theoretical framework to calculate its modes using the network approach is described.

3.1 Network theory

Most of the advancements in physics that have been done in the last centuries focused on systems that are linear, non-interacting, ordered, at equilibrium... However, these situations are far from everyday life, where systems can be non-linear, interacting, disordered, and out of equilibrium. Many interesting features and properties that arise in complex and disordered systems are still waiting to be discovered. Although complexity has been neglected for a long time by physicists, in the past decades complex systems have become a hot topic, so much that a new branch of physics that aims at understanding how complexity can emerge from local and simple dynamics has been established, the Physics of Complex Systems. Increasing interest in how the properties of complex systems are determined by the structure of relationships between elements of the system has been seen in many more fields than just physics. One of the most fruitful theories that has been used by scientists in all disciplines is Network Theory: the study of the relation between the elements of a system and the properties emerging from the topological structure of these relations [23].

Network theory is based upon a branch of mathematics called graph theory, that has as main mathematical objects graphs [24]. A *network*, or *graph*, can be seen as a collection of elements where pair of elements can be related. Each element is called *node* and each pair is called *link*. The term network is usually used instead of the term graph whenever attributes (*e.g.* names) are given to the components of the graph. More rigorously, a graph G is an ordered pair $G = (V, E)$, where V is a set of vertices (also called points or nodes) and $E \subseteq \{\{x, y\} \mid (x, y) \in V^2 \wedge x \neq y\}$ is a set of edges (also called links or lines), which may be ordered or unordered pairs of vertices. Such type of graphs are called *simple*, because they do not allow more than one link between a couple vertices. Graphs that are not simple and allow more links connecting the same pair of vertices need to be defined as $G = (V, E, \phi)$, where V is a set of vertices (also called points or nodes) and E is a set of edges

and $\phi : E \rightarrow \{\{x, y\} \mid (x, y) \in V^2 \wedge x \neq y\}$. If all the edges are unordered pairs of nodes the graph is called *undirected graph*, otherwise if the edges are ordered the graph is called *directed graph*. If the edges carry different weights it is called *weighted graph*. If a graph allows $x = y$ it is called *permitting loops*, as links that start and end in the same node are called loops. An example of simple undirected graph is given in figure 3.1.

The basic key parameters of a network are the number of nodes N and the number of links L . These two parameters show how big and how connected a network is, however are not the only interesting quantities that can be associated to a network. A key property of a single node is its degree: the *degree* k of a node is defined as the number of links attached to it. The number of nodes with degree k is denoted as N_k . The *average degree* $\langle k \rangle$ can be defined as the average of the degree over all the nodes in the network. However, one of the most important features of a network is its *degree distribution* p_k , defined as $p_k = N_k/N$, that gives the probability that a randomly selected node has a certain degree k . The degree distribution varies a lot between networks and is one of the main properties that dictates the behaviours of networks. While some networks have a poissonian-like degree distribution (e.g. the networks that will be used in this work), many relevant networks display a fat-tailed distribution: there is a non-negligible number of nodes with a degree order of magnitudes higher than most nodes. This is the case of protein interaction network or social influence networks.

Another concept that can be defined in a network is the *path length*, that is the number of links in a specific path and the *shortest path distance* d_{ij} , that is the distance between nodes i and j . This is different from physical distance, as it is a property of any type of network (e.g. the distance between two Wikipedia pages can be measured in number of hyperlinks needed to reach the other page). A network is more connected if the average shortest path distance is low. If two nodes are not connected the path length will be $d = \infty$. If all $d \neq \infty$, then the network is *connected*, otherwise it will be *disconnected* and more sub-network *components* or *clusters* will be present.

For most mathematical purposes, the way in which a network is described is through the *adjacency matrix* A . Each element of the matrix A_{ij} stores the relation that the node i has with node j . For a simple network A_{ij} will be equal to 1 if there is a link pointing from j to i and 0 otherwise. If the graph is weighted, A_{ij} will store the weight of that edge. In the case of an undirected network the adjacency matrix will be symmetric, since $A_{ij} = A_{ji}$. The adjacency matrices of real networks are usually sparse networks, i.e. most of the entries of the matrix have value 0. This is due to the fact that usually the degree of the nodes is much smaller than the number of nodes in the system (e.g. even the most popular person on the planet won't be in contact with every other person, but with just a very small fraction). Due to the sparsity of the adjacency matrix, other methods are often employed to store the network computationally (e.g. adjacency list of the connected edges are often used). As an example, the adjacency matrix that represents the network shown in figure

3.1 is

$$A = \begin{pmatrix} 0 & 1 & 1 & 1 & 0 & 0 \\ 1 & 0 & 1 & 0 & 0 & 0 \\ 1 & 1 & 0 & 1 & 1 & 0 \\ 1 & 0 & 1 & 0 & 1 & 0 \\ 0 & 0 & 1 & 1 & 0 & 1 \\ 0 & 0 & 0 & 0 & 1 & 0 \end{pmatrix}. \quad (3.1)$$

Many other topological quantities that determine the properties of a network can be defined. This is the reason why the network approach is so successful: by focusing on the relation between elements of the system and by neglecting unnecessary details, it is able to predict the behaviour of systems of any kind by looking at its topological properties. Network theory has been able to achieve outstanding results in many fields, *e.g.* energy distribution [25], social studies [26] and biology [27, 28].

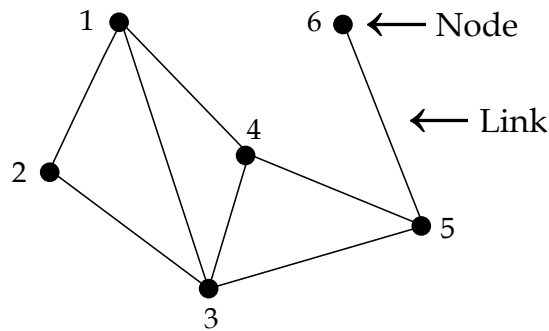


FIGURE 3.1: An example of simple undirected graph. The six nodes are connected between each other by links.

3.2 Network Random Laser

A *Network Random Laser* (NRL) is a random laser where light is confined in randomly placed waveguides connected together at their crossing, arranged as a 2-D graph. The optical feedback is provided by the interference of waves propagating through the links and nodes of the graph 3.2. Undirected graphs can be used to describe and model NRLs. The coordinates of each node can be stored so that the distance between nodes can be retrieved.

In a NRL the complex and multiple interferences of the many recurrent loops can lead to topology-dependent mode formation with high-quality factors or a specific spectral profile. Spatial confinement in a low-dimensional multiple scattering architecture can enhance the interaction of light and promote coupling of emitters. In addition, in a NRL, the scattering strength can be designed changing the connectivity (*i.e.* the number of links and its degree distribution) and light transport can be designed via link length and network size: the decoupling between light scattering and light transport provides an added design advantage. Moreover, the optical modes can be designed by the network topology.

Most RLs, e.g. semiconductor powders or perforated membranes, are usually described either with an independent scattering or coupled-dipole approximation or with a direct numerical solution to Maxwell's equations. Describing light propagation using the graph approach allows a simple and highly effective framework to describe realistic-sized systems accurately, as well as designing the lasing action of a random laser.

Studying mode controllability in a NRL allows us to face the problem both theoretically and experimentally. The controllability of a mode and its relation to the network topology (degree distribution, size, type of network and local features) and the type of mode (mode extension and position relative to the network size) can be easily studied thanks to the network approach. Experimental mode control and selection can be achieved changing the pumping profile: by changing what parts of the link can provide gain the modes that can lase will change too. In principle, with suitable pumping profiles, the spectrum of the laser can be modified as desired. Theoretical calculations can provide useful information about the best types of networks for mode controllability and the best way to experimentally control it.

In this work, the emphasis is put on the selection of a single wavelength from the NRL spectrum, finding the specific pumping profile that favours the selected mode.

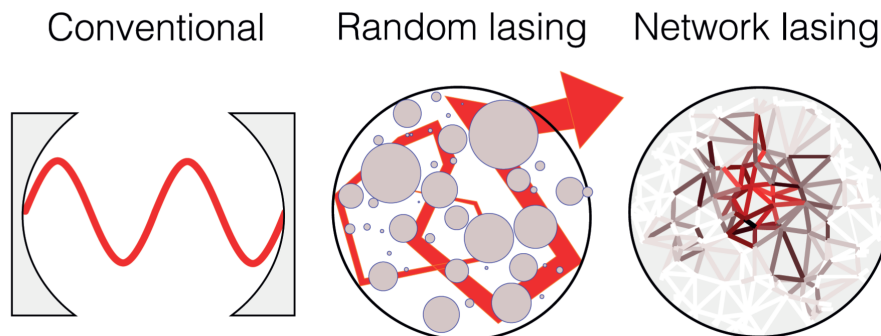


FIGURE 3.2: In random lasers optical feedback is provided by scattering particles, instead of reflective surfaces or distributed periodic structures. In network random laser the modes of the laser are formed by the interference of waves propagating through links and nodes of the graph.

3.2.1 Calculating the modes of a NRL

The theoretical framework used to calculate the modes of a network is here explained. The approach that will be adopted is the one described by Michele Gaio [4]. In order to calculate the modes of the network Maxwell's equations are solved on a graph [29]. As a simplified model we consider the scalar wave equation since a fibre admits ~ 1 -D propagating modes with a defined k . Multiple scattering is described as a boundary condition that waves need to satisfy at each node. We assume that only one fibre mode is present in the link due to the sub-wavelength diameter of the fibre; therefore, light propagation from node i to node j along the link of length L_{ij} that connects them can be

described by the phase acquired by the electric field $E(x_j) = E(x_i)e^{ikL_{ij}}$. The only losses considered are the one at the end of the network; out-of-plane scattering losses at nodes are ignored, as they are computationally challenging to include.

Let's consider a graph with nodes $i = 1, \dots, n$ and edges $r = 1, \dots, N$. The 1-D scalar wave equation that is it going to be solved is

$$\frac{\partial^2 E(x, t)}{\partial t^2} - v^2 \frac{\partial^2 E(x, t)}{\partial x^2} = 0, \quad (3.2)$$

where $v = c/n$ is the speed of light in the fibre with effective refractive index n of the only mode. On each edge the solution of the wave equation in the Helmholtz form

$$\frac{\partial^2 E(x)}{\partial x^2} + k^2 E(x) = 0, \quad (3.3)$$

where $k = \omega/v$, are of the form

$$E_r(x, k) = B_r^+ e^{ikx} + B_r^- e^{-ikx}. \quad (3.4)$$

Since the graph has N edges, there will be N equations of this type with $2N$ coefficients $X_{1, \dots, N} = \{B_1^+, \dots, B_N^+, B_1^-, \dots, B_N^-\}$ that define the behaviour at the nodes. Neumann boundaries condition [30] ensures that energy is conserved at each scattering node:

$$E_r(x_i) = E_s(x_i) \quad (3.5)$$

for all edges r and s connected to the node i , and

$$\sum_r \left. \frac{dE_r}{dx} \right|_{x=x_i} = 0 \quad (3.6)$$

for all edges r connected to the node i . Given a certain k , these conditions can be put in a $2N \times 2N$ sparse matrix $M(k)$, so that

$$M(k) \cdot X = 0. \quad (3.7)$$

The eigenvalues of the system are therefore found by computing

$$\det(M(k)) = 0. \quad (3.8)$$

This approach can be implemented numerically. The graph is defined by a $n \times n$ adjacency matrix A , where n is the number of nodes, and by a vertexes array $V = \{(x, y)_r\}$ with $r = 1, \dots, N$. The edges can be labelled as $(i, j) \iff r$, with $i, j = 1, \dots, N$ and $j > i$, and the coefficients of X will be B_{ij} . Therefore, the solution in each edge can be written as

$$E_{ij}(x, k) = B_{ij} e^{ikx} + B_{ji} e^{ik(L_{ij}-x)}, \quad (3.9)$$

where L_{ij} is the length of the edge and $x \in [0, L_{ij}]$. The boundary conditions at each node are

$$B_{ij} + B_{ji}e^{ikL_{ij}} = B_{li}e^{ikL_{il}} + B_{il}, \quad \forall j, l \mid (A_{il} \neq 0 \wedge A_{ij} \neq 0), \quad (3.10)$$

$$\sum_{l < i} (B_{li}e^{ikL_{ij}} - B_{il}) + \sum_{l > i} (B_{il} - B_{li}e^{ikL_{il}}) = 0, \quad \forall l \mid A_{il} \neq 0. \quad (3.11)$$

An edge can be left open at one end by imposing no reflection at that node (e.g. $B_{ij} = 0$ for open end at node i). Equations 3.10 and 3.11 can be written using two matrices M_0 and P that do not depend on k , and the element-wise product \odot :

$$M = M_0 \odot e^{-ikP}. \quad (3.12)$$

Since M is sparse, the eigenvalues can be easily computed for large number of nodes. Numerically, the values of k for which the matrix is singular are identified estimating the condition number C of $M(k)$ (`cond` function in the MATLAB code described in the following section) on a grid of the complex k region of interest and finding the maxima of C . The located guesses for k are optimized (simplex search) until convergence. The real part of k is related to the wavelength of the mode; the imaginary part of k is related to the loss of the mode.

Chapter 4

Numerical simulations of NRL

In this chapter the lasing behaviour of a NRL is studied using a computational approach. The modes of a network are calculated and an adaptive pumping procedure is simulated in order to understand which procedure can be used experimentally.

4.1 Mode selection code

A MATLAB code developed by Michele Gaio at Imperial College London is used to calculate the modes of networks ($\text{Re}(k)$, $\text{Im}(k)$, and intensity distribution of the mode across the network). The networks analyzed are generated either with a code by Michele Gaio, for Buffon-type networks [31], or manually. The computational cluster of Math and Physics Departments of Imperial College London has been used for the calculations. Each simulations takes few dozen of minutes to be completed.

A python code has been written to simulate the selective pumping of the network. The aim of the code is to study the controllability of different networks for different modes, as well as defining an experimental procedure that can be used to select a mode with the least number of iterations.

Lasing action is achieved when the losses of the mode are compensated by the gain provided by the medium. When the network is not lasing a linear approximation to the problem is valid and each link will provide gain proportionally to the energy of the optical pump. How the gain is divided between modes represents a critical point: the code calculates the field intensity of each mode across each link of the network, however values between different modes cannot be compared since they are not using the same units. Even so, as long as the losses are small (small $\text{Im}(k)$) we can normalize the sum over all links to 1 for all modes; for modes with higher losses such approximation is not valid, but since the sum over all links is going to be smaller than 1 they are going to be neglected. In the approximation used in this project the lossier half of the modes is neglected. The gain $g_{i,l}$ that a mode i will get by pumping a link l is

$$g_{i,l} = \frac{I_{i,l}}{\sum_j I_{j,l}} \cdot L_l \cdot \Gamma, \quad (4.1)$$

where $I_{i,l}$ is the normalized intensity of the mode i in the link l , L_l is the length of the link l , and Γ is the total gain that a unit length of link provides when shined with a beam, that is proportional to the energy of the beam.

The value of Γ can be assigned arbitrarily, given that we don't know the exact relation between total gain and energy of the beam. An arbitrary value that allows lasing in as many modes as in an experimental NRL (~ 20) when an experiment-like network is fully pumped is used. The value of Γ is expressed in appropriate units that allow the gain $g_{i,l}$ to be in the same units of $\text{Im}(k)$, so that if the sum between the two terms is greater than zero the mode is lasing.

The routine that selects a single mode works similarly to the experimental one (see section 5.1). The network is initially fully pumped and one of the lasing modes is selected to be maximized. Single links of the network are individually not pumped (or switched *OFF*) and the new spectrum is compared with the previous one: if this action (or *move*) favours the selected mode the link is kept *OFF*, otherwise it is switched *ON* again. This procedure is repeated for all links.

There are two main issues that can change the speed and effectiveness of the code: the order in which links are tested; the function to decide whether a new move should be accepted or not. Three different ordering of link priority have been tried: random order, closeness to the center of the network, and closeness to a ring centered in the center of the network of variable radius. The function \mathcal{G} to evaluate moves is the sum of more contributions from few other functions. One class of functions \mathcal{A}_N calculates the ratio between the height of the selected peak and the average height of the N highest peaks apart from the selected one before and after the move, calculates the ratio between them and subtracts 1: values higher than 0 show that the selected mode is favoured with the new pattern; the height is referred to a base value arbitrarily chosen as the lossier mode's $\text{Im}(k)$. A second function \mathcal{B} is used to avoid having the selected mode decreasing in intensity too significantly and it is equal to $-b/I_k^c$, where b, c are an arbitrary positive constants and I_k is the height of the selected mode k with links l_i *ON* referred to 0 ($g_{k,l_i} + \text{Im}(k)$ without base value). If the value of the function \mathcal{G} is greater than 0 the move is accepted.

In order to check the mode optimization speed some parameters ζ_n are calculated at each step. The parameters ζ_n are equal to ratio between the height of the selected peak and the average height of the n highest peaks apart from the selected one. This parameter is not to be confused with the \mathcal{A}_N functions used in the \mathcal{G} function.

4.2 Results of the numerical simulations

The code has been tested on Buffon-type networks – networks created by randomly placing straight lines on a plane. The results of mode selection shown here refer to one specific network chosen as example, although the code has been checked for few different networks. The results were similar for all checked networks. The modes of the network are calculated and shown in figure 4.1 and 4.2. The network is fully pumped and the gain is added to each mode, as shown in figure 4.3. The optimization code is run using as link ordering the closeness to a ring centered in the center of the network of radius

30% of the network size. The chosen acceptance function is $\mathcal{G} = \mathcal{A}_3 + \mathcal{B}(b, c)$ with $b = 1000, c = 1$ (used for all the tested networks). These choices were made after testing the code few times on these type of networks and looking at the best results. The selected modes were the first and second highest modes. Results are shown in figure 4.4, 4.5 and 4.6.

In order to check the speed and performance of different mode selection procedures the control parameters ζ_n can be checked at every optimization step and the acceptance ratio (number of accepted moves out of total number of moves, here calculated every 10 moves) throughout the procedure can be compared. The results can be see in figure 4.7 and 4.8 (with $n = 1, 3, 10$).

The results for the same network with same acceptance function but random link ordering, optimizing the highest mode only, are presented in figures 4.9, 4.10 and 4.11.

The procedure is then run using the initial ring ordering and acceptance function $\mathcal{G} = \mathcal{A}_N + \mathcal{B}$ with N ranging from 1 to the number of calculated modes minus one. Control parameters ζ_n and the total percentage of accepted moves are calculated at the end of each simulation. The results are shown in figure 4.12 and 4.13.

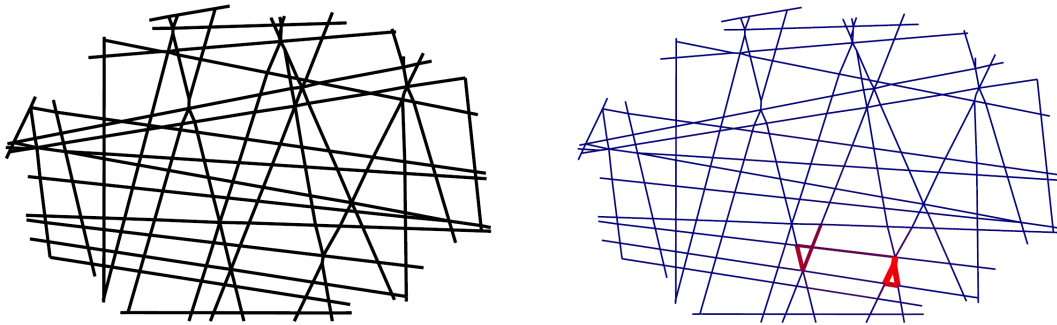


FIGURE 4.1: Left: image of the network used for the simulation. Right: example of the field distribution of a mode in the network. Thicker and red links have a bigger field intensity. The mode here displayed is the first highest after full pumping.

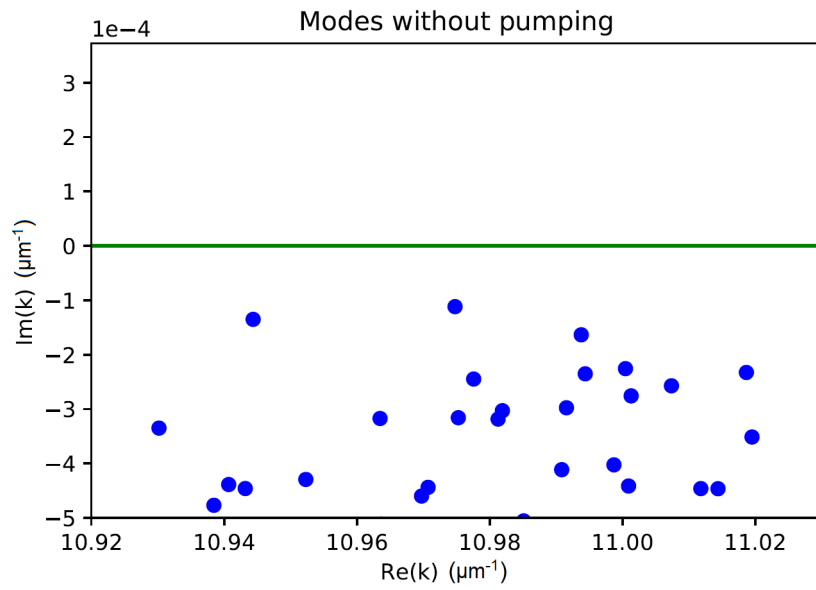


FIGURE 4.2: Modes of the network without any pumping. All modes have a negative $\text{Im}(k)$ since there are only losses in the system and no gain is provided.

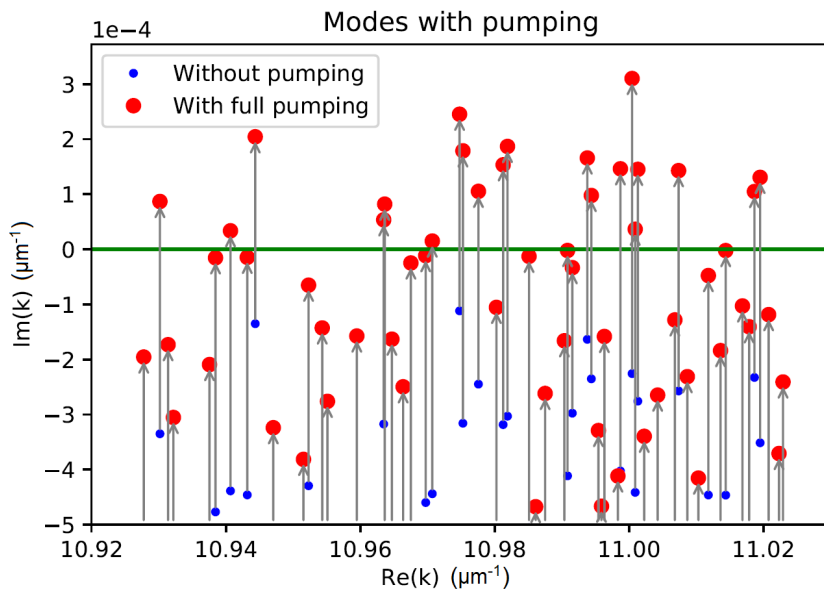


FIGURE 4.3: Modes of the network with all the links of the network pumped. Various modes are above threshold. The first and second highest modes will be used as selected mode for the optimization procedure.

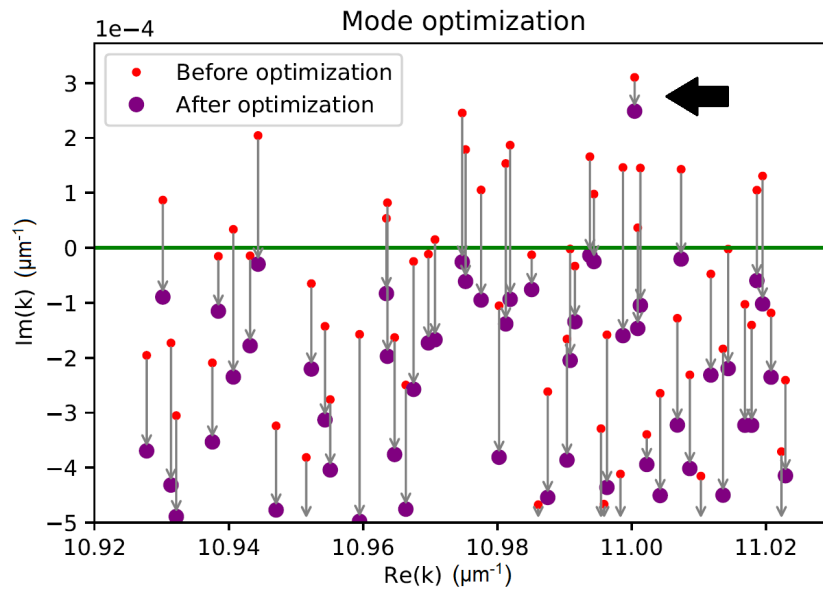


FIGURE 4.4: Modes of the network after mode selection procedure for the first highest mode at full pumping. Only one mode is above threshold. The optimized peak is indicated by the arrow.

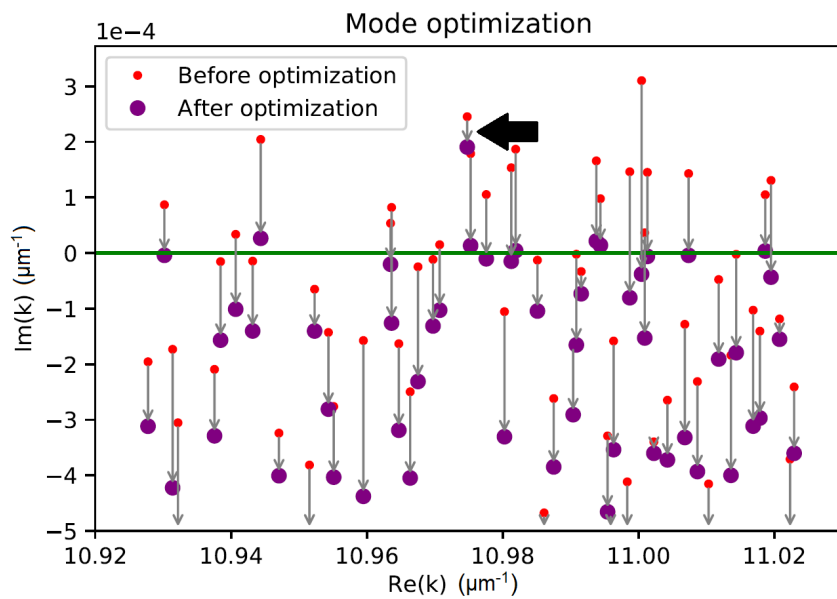


FIGURE 4.5: Modes of the network after mode selection procedure for the second highest mode at full pumping. Only few modes are above threshold. The optimized peak is indicated by the arrow.

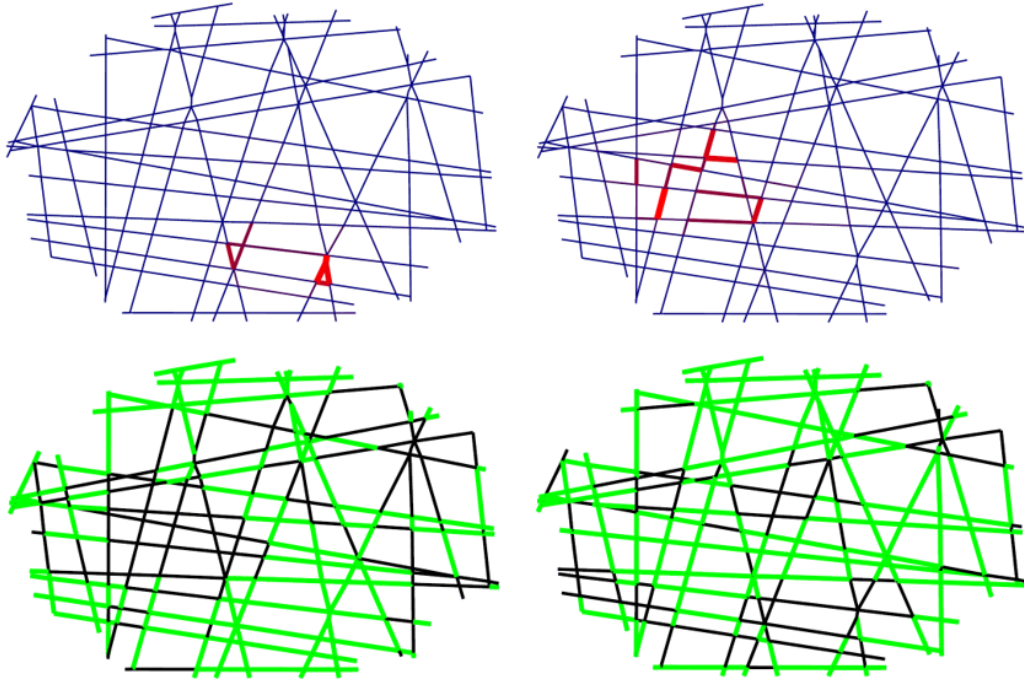


FIGURE 4.6: The field distribution of two modes are shown on the top half (left for first highest, right for second highest). The illumination patterns for each of the two mode selection procedures are shown on the bottom half. As expected, links where the mode is more intense are ON for the pattern that optimizes it, while are OFF for the other one.

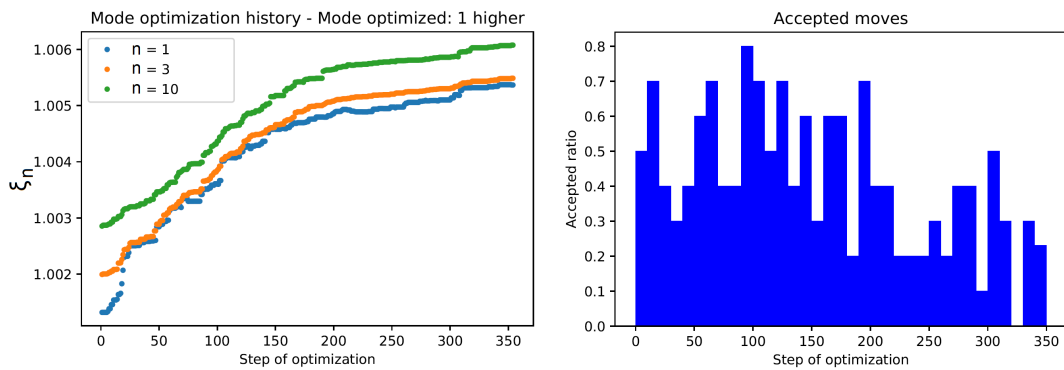


FIGURE 4.7: Image regarding the first highest peak. Left: Control parameters ξ_n at every optimization step. Right: fraction of accepted moves every 10 moves.

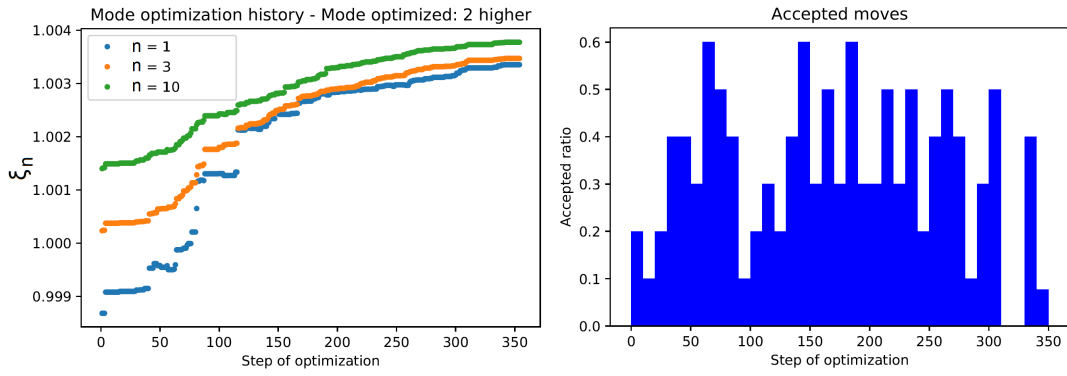


FIGURE 4.8: Image regarding the second highest peak. Left: Control parameters ζ_n at every optimization step. Right: fraction of accepted moves every 10 moves.

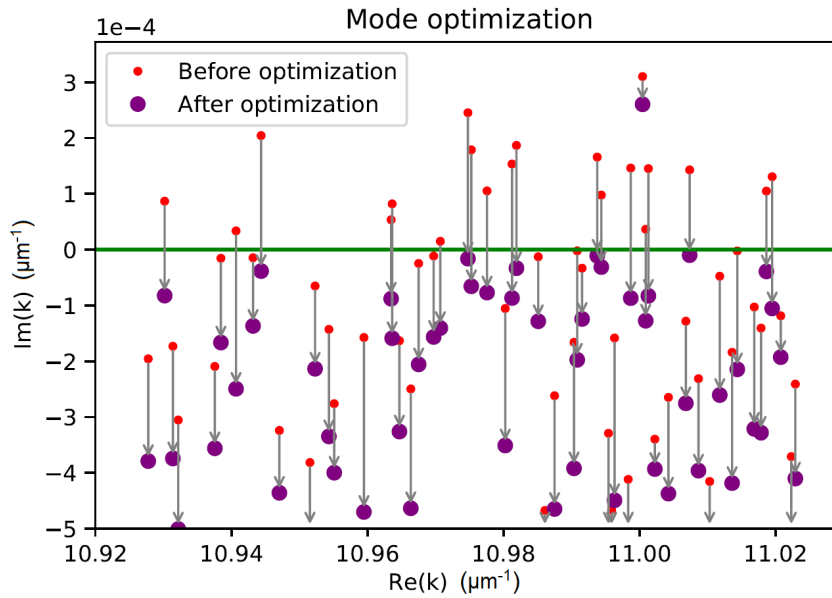


FIGURE 4.9: Modes of the network after mode selection procedure for the highest mode at full pumping with random link ordering. Only one mode is above threshold, as in figure 4.4, although the decreases in $\text{Im}(k)$ are not identical.

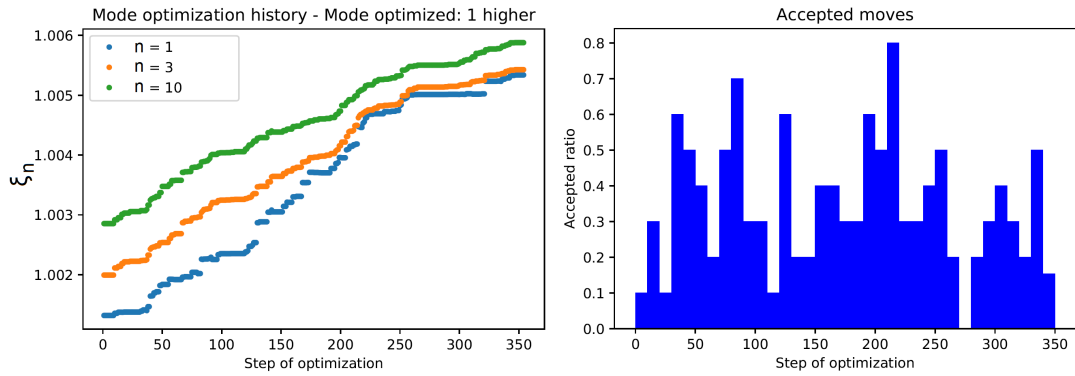


FIGURE 4.10: Image regarding mode selection with random link ordering. Left: Control parameters ζ_n at every optimization step. Right: fraction of accepted moves every 10 moves.

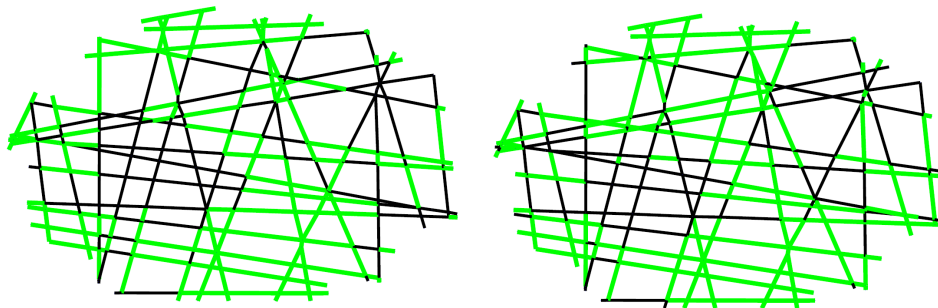


FIGURE 4.11: Illumination pattern after mode selection procedure: with ring ordering on the left side, with random link ordering on the right. Between the two found configurations only minor differences are present.

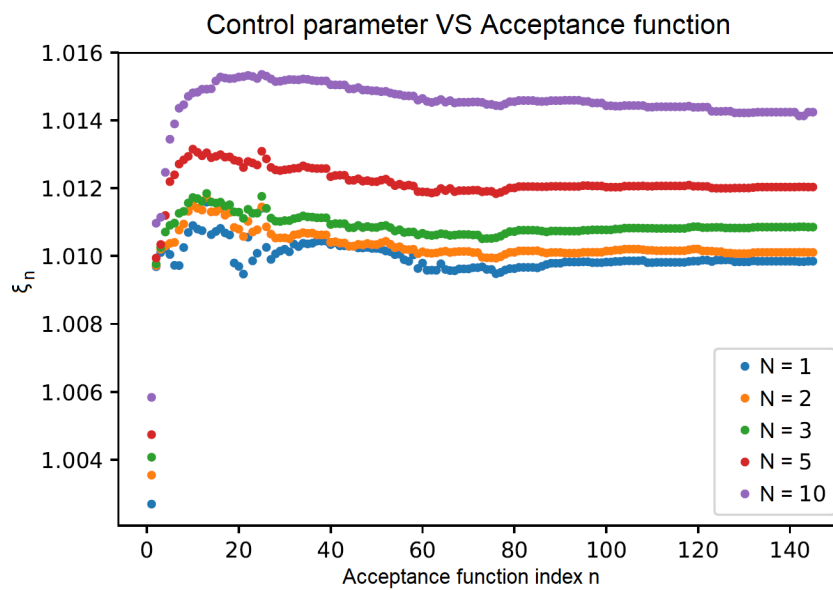


FIGURE 4.12: Control parameters ζ_n at the end of optimization procedure with acceptance function \mathcal{A}_N with varying N .

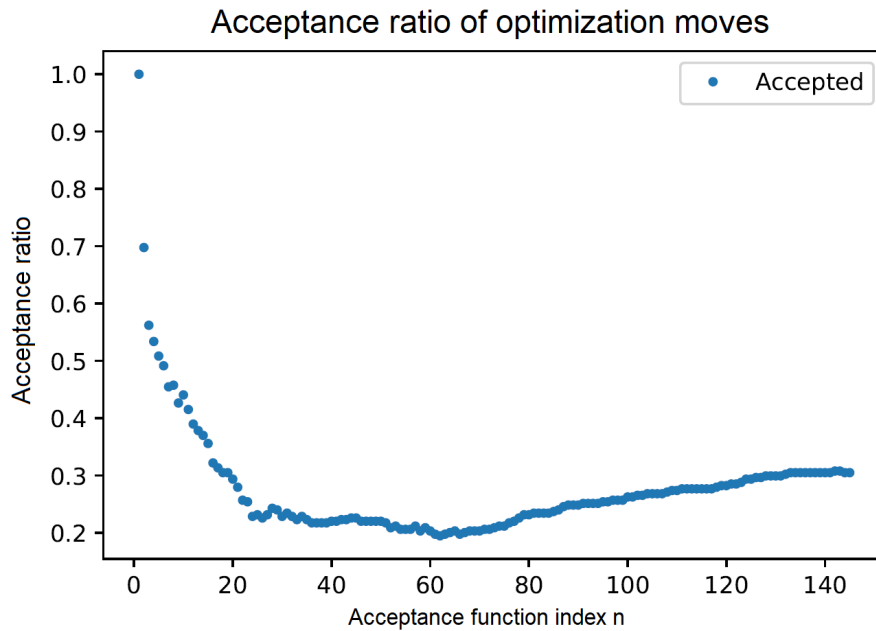


FIGURE 4.13: Fraction of accepted moves at the end of optimization procedure with acceptance function \mathcal{A}_N with varying N .

4.3 Discussion of modeling results

The theoretical model is not reliable when modes are above threshold, since the system does not behave linearly after lasing. However, the procedure is still valid since the final configuration has just few modes above threshold and the exact behaviour of single modes during the procedure is not important.

The illuminated links are also the ones where the selected mode has higher intensity compared to the other modes, as seen comparing figures 4.1 and 4.11. Such result is expected, since switching off those links would only favour other modes.

Choosing which is the best optimization procedure is not trivial. One needs some parameters to quantify how the procedure performed, as well as how good one optimized spectrum is compared to another optimized spectrum. The control parameters ζ_n measure the height of the selected peak compared to the following n highest peaks. However, there is no correct value n to choose, therefore few values of n in the range 1 to 10 are checked. Higher values of n are not useful since they take into account modes that are already very low and cannot be experimentally detected; low values of n are not meaningful alone since the selected mode needs to suppress all other modes.

A good link ordering should exhibit a quick growth in the control parameters ζ_n over the optimization steps. In this case, the most important links for the mode optimization are checked first, leading to convergence sooner. Such feature is very important for the experimental realization of the procedure. Moreover, it has been noticed that higher values of ζ_n are reached when ζ_n increases during the first optimization steps. However this relation needs to

be verified with a bigger sample. Another feature of a good link ordering is a high acceptance ratio during the first phase of optimization.

The most important modes are usually localized near the center of the network, therefore ordering links by the distance from the center or from a ring should have better performances than a random ordering. This is verified looking at the different slope of ξ_n and acceptance ratio in the two cases (figures 4.7 and 4.10).

A good acceptance function \mathcal{G}_N should achieve the highest values of ξ_n with the smallest number of accepted moves for all networks. Patterns with few links ON are not likely to lase in the experiment, therefore low number of accepted moves are preferred. The function \mathcal{B} prevents the selected peak from getting to close to threshold and contributes to rejecting moves that are not as good as other ones.

Different values for N have been studied for the function \mathcal{A}_N . From figure 4.12 it can be seen that values of N between 3 and 20 have the highest ξ_n . The control parameters are very low for $N = 1$ but increase quickly for higher N values: optimizing using just the second highest peak is not as efficient as using more peak. This is not surprising, since the selected mode needs to suppress all other modes, not just the next highest one. The control parameters decrease for higher values of N : very lossy modes do not need to be taken into account.

Figure 4.13 shows that fraction of accepted moves with different N values. The number of accepted moves diminished rapidly below 50% after $N \sim 5$. This is the reason why $N = 3$ was chosen: the control parameters were only slightly lower than the ones with higher N , but the number of accepted moves was significantly higher.

A major goal of the mode selection procedure is to find a good starting point for the experimental counterpart procedure. The spectrum has no fluctuations in the simulation, therefore the experimental code must take this issue into account while not increasing the number of pulses shot to the sample.

A limitation of this model comes from the fact that it is not able to take into account consistently the losses at each node that happen experimentally due to scattering. Such phenomenon is important in real-life samples and may play a major role in mode controllability in NRLs. Therefore, this model is useful to provide a starting point for the experiment and to more realistic models to be developed.

Chapter 5

Experimental part

In this chapter the lasing behaviour of NRL samples is checked and mode controlling on such samples through adaptive pumping is studied experimentally using a similar procedure to the one suggested in 4.2.

5.1 Methods employed in the experiment part

5.1.1 The experimental NRL sample

The nanophotonic networks consist of subwavelength waveguides connected together at their crossing. They are fabricated by electrospinning single-mode polymethyl methacrylate (PMMA) polymer nanofibres (diameters in the range 200-500 nm) doped with a laser dye, Rhodamine-6G, with a concentration of 1% wt:wt relative to the polymer matrix. The fibres are deposited on a strip with TEM support grids on top (with 425x425 μm opening, by TAAB Laboratories Equipment Ltd.): this is to avoid that the fibres touch the surface of the strip. These regions, where the fibres are suspended and therefore do not lose light into the underlying strip, are the one used for the experiment. The network degree d is in the range 4 to 6, with average degree $\langle d \rangle = 4.4$, average link length $\langle l \rangle = 26.5 \mu\text{m}$ and around 200 nodes. The samples are created by an external lab [32]. An image taken with the spectrometer of a typical area in the sample is shown in figure 5.1.

Rhodamine-6G is a dye that has an exceptionally high photostability, high fluorescence quantum yield and low cost, with a lasing range of 570 to 660 nm with a maximum at 590 nm [33]. Such properties explain why this material has been chosen as active medium.

Electrospinning is a manufacturing technique involving an electrohydrodynamic process used to create electrospun fibres from a polymer solution [34]. Usual setups for this technique include the following components: a solution contained in a reservoir that ends with a spinning tip; a pump; a high voltage power source; a collector. In order for the spinning process to start, a voltage is applied to create an electric field between the needle tip and the collector while the solution is pumped at a constant flow rate. The electrostatic repulsion on the liquid surface becomes so intense that a cone forms instead of a meniscus and the charged liquid jet is ejected towards the collector. The collector is a surface where the fibres deposit; it can be stationary, moving or rotating. One of the main advantages of the electrospinning technique is

its versatility of processing to create fibres with multiple arrangements and morphological structures.

The width of the fibres is an important parameter: if they are too thick the fibres would not be single-mode fibres, as higher orders would not be negligible; if it is too thin most of the field would be outside of the fibre and losses would be massive. PMMA fibres created with electrospinning have the right thickness that enables the spontaneous emission to couple to the fundamental waveguide mode in these subwavelength fibres with an efficiency as high as 30–50% [35]. The losses of the system are inherently high.

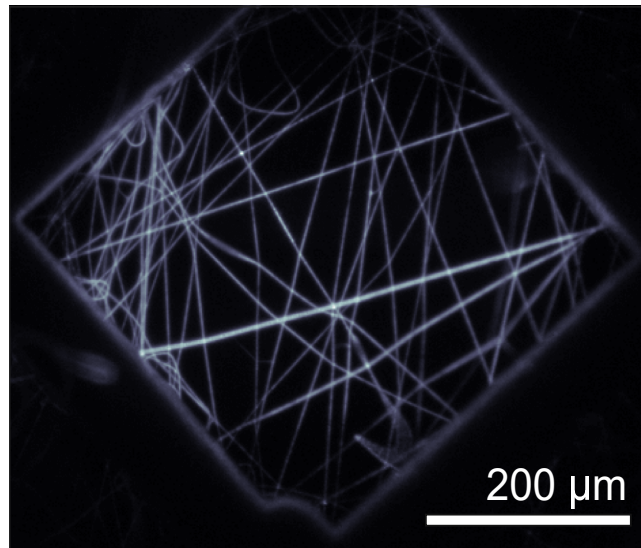


FIGURE 5.1: Image of a typical area within a sample. The TEM grid holds the fibres so that they do not touch the underlying surface.

5.1.2 Experimental setup

The main components of the experimental setup are:

- Pulsed laser of $\lambda = 532 \text{ nm}$ – TEEM Microchip, pulse width $\sim 500 \text{ ps}$, spot diameter $\sim 160 \mu\text{m}$. The typical energy of a pulse is $\sim 20 \mu\text{J}$, measured right after the output aperture.
- Acousto-Optic Modulator (AOM) that allows to change the energy of the pulse electronically. Values between 0 and 5 V are used to change the energy of the pumping laser from 0% to 100% respectively. Some beam stoppers must be placed on the optic table in order to block higher orders produced by the AOM.
- Digital Micromirror Device (DMD) that allows to change the wavefront shape – Ajile DMD4500 with 912×1140 mirrors. Any black-and-white image of 912×1140 pixels can be sent to the DMD to be displayed and change the beam profile. The shape of these mirrors is rectangular, therefore, in order to have a square illumination pattern of side n the

instruction image will need to have a $n \times 2n$ rectangle. We will therefore say that the DMD has 912×570 "effective pixels", as these are the numbers that are relevant if we want to divide the illumination profile into squares. A picture of the DMD is shown in figure 5.2.

- Confocal microscope with various objectives (only the $\times 10$ was used). The sample can be moved along all three axes. A white light source is placed on top of the sample holder. In figure 5.3 a scheme shows how the microscope serves both to focus the pump light and to collect the light from the sample.
- Grating spectrometer IsoPlane SCT320 Princeton Instruments equipped with a 1800 gr mm^{-1} holographic grating (0.025 nm resolution): changing the aperture of the slit either the spectrum or the full image of the sample can be acquired. A green filter is placed in front of it to stop the pump laser light and allow only the light emitted by the sample to be detected. In order to acquire the spectrum the slit aperture is narrowed to have more defined peaks, so only the spectrum from a section of the sample is taken.
- stage where lenses to change the beam size to achieve an uniform illumination of the sample can be placed.
- CCD camera (Princeton Instruments Pixis 400) for white light measurements and coarse alignment.

The experimental setup is illustrated in figure 5.4. Such setup allows the sample to be illuminated with different pumping patterns (thanks to the DMD) and different pumping powers (thanks to the AOM) with various illumination frequencies that can be synchronized with the spectrometer data acquisition and DMD pattern display. A pulsed laser is used instead of a continuous one to avoid photobleaching the sample while achieving lasing. Pulse energy is measured using a laser energy meter, that can also evaluate RMS and PTP stability over up to 1000 measurements. The laser light in the system is detected through the scattering at the nodes, since it is not possible to measure the laser output at the margins of the network in this experimental setup.

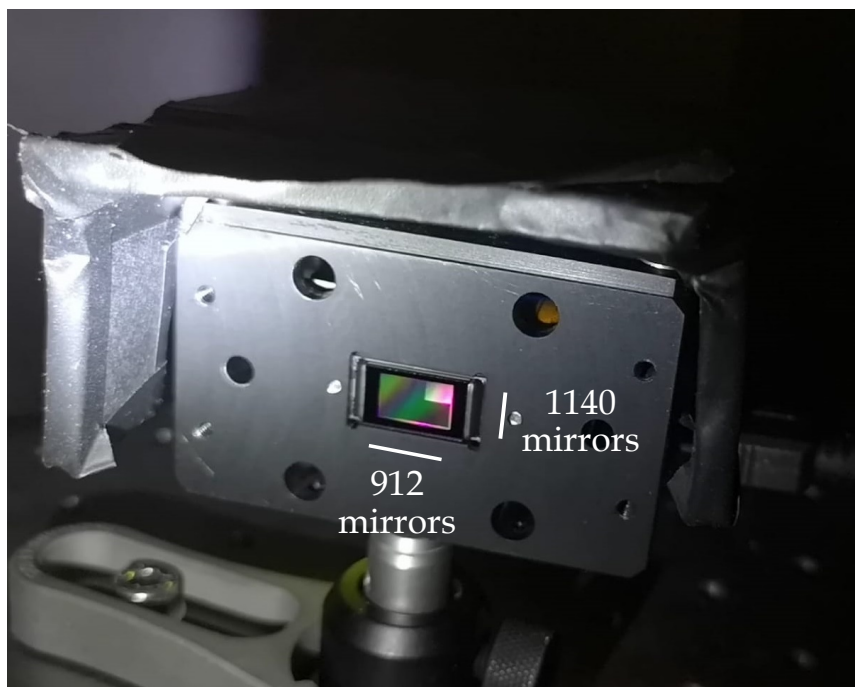


FIGURE 5.2: Picture of the DMD, taken while displaying a pattern with a single box of illumination. Notice that the highest number of mirrors is in the shorter side.

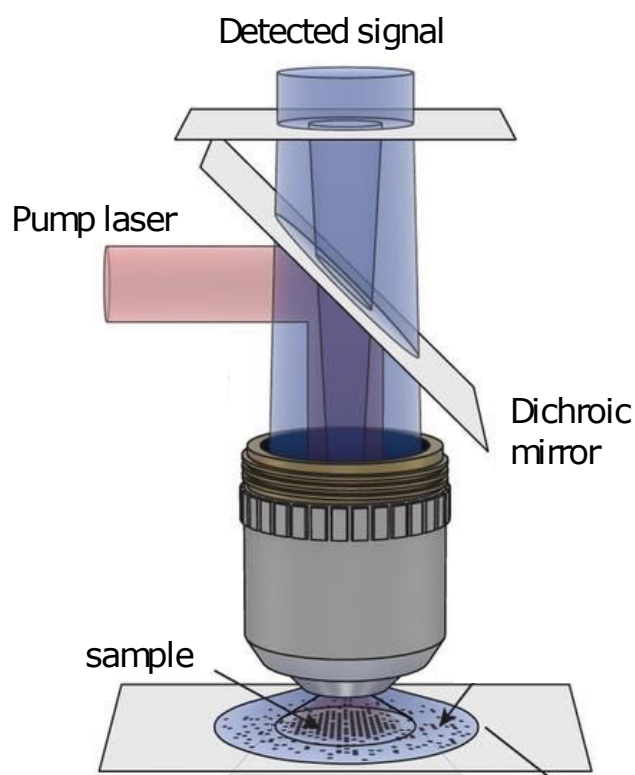


FIGURE 5.3: This scheme explains how the sample is pumped by the pump laser light and how light from the sample is collected. A filter for the pump laser wavelength is put in front of the spectrometer.

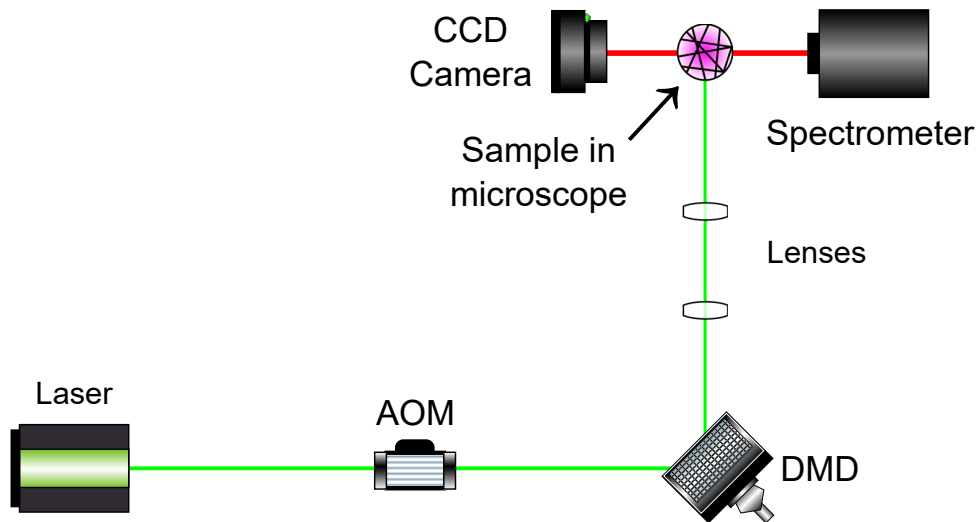


FIGURE 5.4: The experimental setup is represented with this simplified scheme. The AOM varies the energy of the laser pulses. The DMD changes the transverse section of the beam. Lenses are put before the microscope to change the beam size. Light from the sample is collected by either a CCD or a spectrometer.

5.1.3 Experimental mode selection routine

The aim of the project is to find a procedure that is able to find a pattern that selects the wanted modes, either by suppressing all the other modes, or by enhancing the selected ones. However, even if we have a network with 40 links – or we use a 8×5 illumination chessboard – the number of possible configurations is $2^{40} \simeq 10^{12}$. Not only it would be unfeasible to test all these configurations, but due to photobleaching-related effects the number of configurations that can be visited must be reduced to the bare minimum. An effective procedure must be able to arrive to one of the possible configurations that favours the selected modes in the minimum number of moves. The approach that has been taken is reminiscent of the steepest descent method, that is one of the simplest and fastest one. Other methods, such as genetic algorithms or simulated annealing, are able to arrive at solutions closer to the global minimum, but usually need a higher number of moves.

A code in python and Matlab for mode selection has been built. Using the DMD the illumination field of the laser is divided in a chessboard pattern of size $N_1 \times N_2$, (usually $N_{1,2} \sim 5 - 20$), where each square can be illuminated or not (ON/OFF). Using a chessboard instead of trying to illuminate single links in a network is chosen as it is much easier to implement. Starting from an all-ON pattern, single squares are switched off (this action will be also referred as *move*) and the resulting lasing spectrum is compared with the previous one: if this change favours the mode that we want to select, that area is kept OFF, otherwise is switched back ON. This procedure is repeated for all squares. The whole process can be repeated again starting from the final pattern instead of the all-ON pattern; the same chessboard division can be used, otherwise

a finer chessboard of size $M_1 \times M_2$, with $M_{1,2}$ multiple of $N_{1,2}$ can also be chosen.

There are two main issues that can change the speed and effectiveness of the code: the order in which squares are tested; the function to decide whether a new move should be accepted or not. In this code the chosen square order is given by the distance from the center of the pattern, as suggested by the numerical simulation (see section 4.3). The function calculates the ratio between the height of the selected peak and the average height of the following N_p highest peaks before and after the move: if the ratio after the move is higher than the move is accepted, otherwise the move is refused and the square is switched on again. Such function and its value is referred as *cost function* or *optimization parameter* ζ_{opt} :

$$\zeta_{\text{opt}} = \frac{I_{k^*}}{\sum_{i=1}^{N_p} I_i / N_p}, \quad (5.1)$$

where I_{k^*} is the intensity of the selected mode and I_i is the intensity of the i^{th} most intense mode, excluding the selected one. The chosen value of N_p is 10, as suggested by numerical simulations (see section 4.3) and preliminary measurements. The most intense modes cannot be found by sorting the data bins by number of counts, since bins next to a maximum may be higher than other peaks but should not be taken into account; therefore, bins next to a maximum are not used to find the highest peaks.

The program also allows to choose whether to optimize the n^{th} highest mode, a specific frequency, or more than one mode (*e.g.* the two highest modes): in the latter case the function that decides if a new move should be accepted or not uses the average of the chosen peaks instead of a single height.

The program takes into account possible shifts in the spectrum of the peaks (see section 5.2.3): this is done by setting a variable that, by checking at every iteration the shift in position of the highest peak, is the sum of the shifts at every iteration: if the sum is greater or equal to 5 in absolute value, the position of the peak is updated by shifting it by one bin. Such method avoids shifting the peak due to fluctuations since a threshold needs to be reached and the shift can be reverted.

5.1.4 Experimental procedure

The experimental procedure to shine and study the sample is now described. A fluorescent film is placed on the microscope sample holder. The laser is turned on, its power and stability checked, and the system aligned. In order to align it, the emission of the fluorescent film is checked in far field using the CCD, adjusting the various parts of the setup in order to achieve a uniform circular beam profile on the film. A calibration slide is used to get the conversion between pixels and μm of the sample image. Then, the sample is placed on the microscope sample holder. The sample top side is first moved coarsely towards a suitable area of the sample, then into the focal position using the CCD; the position is finely tuned using the spectrometer (setting the

spectrometer aperture wide open). The laser power is controlled by changing the voltage on the AOM through a LabView program. Data acquisition is controlled via a Matlab program. The background spectrum is always taken at the beginning of data acquisition and subtracted to the data. The acquisition wavelength range of the spectrometer is changed accordingly to the spectrum of each area.

The L-L curve (input power VS output power) is first taken to check the lasing behaviour of the studied area of the sample. If the studied area is promising, the mode selection code is run few times until a satisfactory spectrum is achieved or if the lasing spectrum turns out to be too unstable or weak.

For each illumination the actual number of pulses sent to the sample is 5. These pulses are sent one after the other while the spectrometer is acquiring the spectra. This provides a higher number of counts, as well as a measurement that is less affected by the laser pulse to pulse differences. This is possible since *Random lasing process typical time scale* \ll *Input laser pulse length* \ll *Time between pulses* \ll *Spectrometer acquisition time*. The time between each illumination is around 2-3 seconds, so an optimization with 160 moves takes around 6-8 minutes to be completed.

The typical energy of a pulse is $\sim 16.0 \mu\text{J}$ before entering the AOM and around 10% of that value at the sample – after AOM (set at 5 V), an all-ON pattern on the DMD and various lenses. Typical RMS stability values measured before the AOM are around 2.5%, while PTP stability values are around 5%.

5.2 Results in the experimental part

The experimental results are here shown and discussed. The results have been divided in: preliminary measurements; non-linear behaviour; mode selection issues and results.

5.2.1 Lasing behaviour check and preliminary measurements

Two set of samples have been checked for lasing action: a new set and an old set. The new set has been checked to verify that it has been manufactured correctly; the old set has been checked to see if photobleaching damaged the sample or if it is still working.

The new set of samples has 4 samples with different link density. Images of the samples taken with white light are shown in figure 5.5. Lasing from the sample has been checked using different laser powers and shining different parts of the samples. There are no spikes in the spectra even with maximum energy, therefore no lasing activity is seen. The results for the new sample are shown in figure 5.6 and figure 5.7. The geometry, link density, and degree of links were promising, but lasing was not observed even at the highest pumping power. Thanks to figure 5.7 it is possible to state that the absence of lasing is not due to a low pumping power, but it is intrinsic of the sample: the

saturation of the fluorescence of the sample is a clear sign that almost all dye molecules in the sample are used. It is probable that a problem with the dye or the fusion between links is causing the sample to not lase. These data have been sent to the sample-maker research group for further investigation.

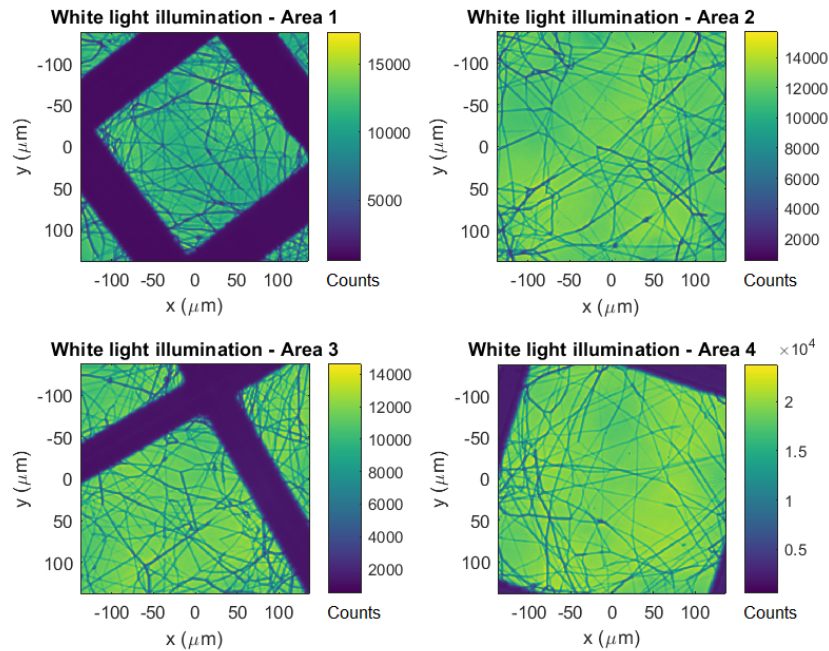


FIGURE 5.5: Images of the studied areas in the new set of samples taken with white light.

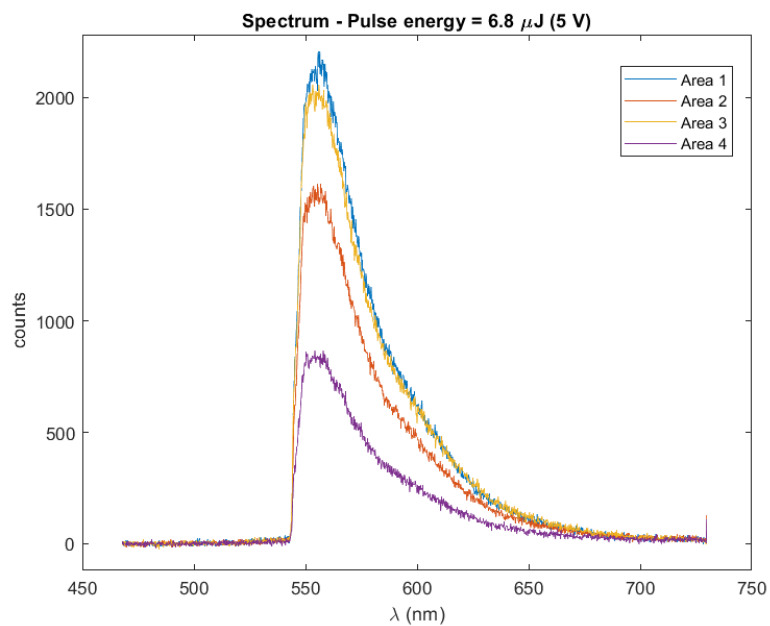


FIGURE 5.6: Spectra at full pumping power from different areas of the sample. No lasing peak is present.

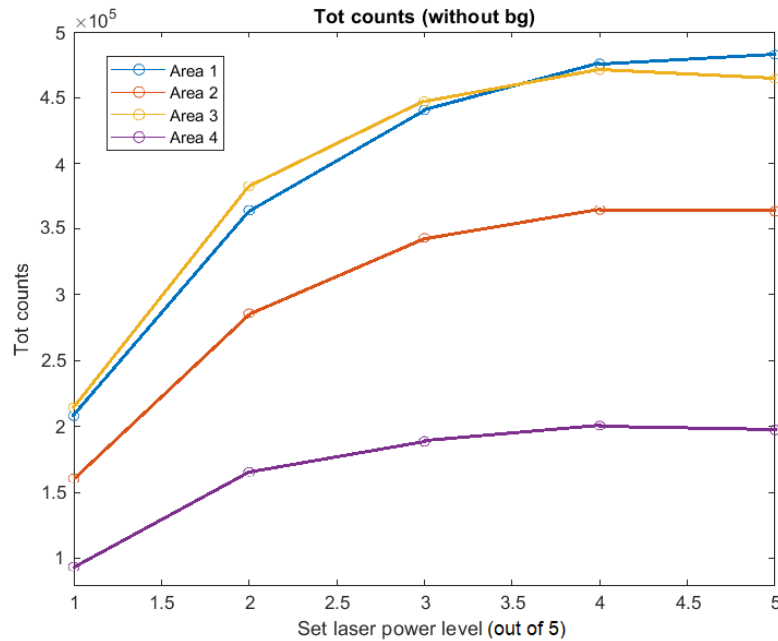


FIGURE 5.7: Total counts from each area at different pumping powers. Saturation can be seen at high power in every studied area of the sample.

The old sample showed lasing in the past, however photobleaching could have damaged the sample causing it to not lase again; therefore, the sample is checked. A very fibre-rich area is first checked. Lasing activity can be seen by the presence of a peak in the spectrum. The mode selection routine is run on the sample to check if it is a feasible area to optimize a peak. A chessboard pattern of size 3×4 is used in the first part and a 6×8 in the second one. The code succeeded in isolating a mode in one area of the sample. The results for the new sample are shown in figure 5.8 and figure 5.9. The spectrum of such area does not display many isolated peaks, probably due to the presence of many links in this area. The optimization procedure can only use the absolute values of counts, not the relative number of counts with respect to the incoherent background. Therefore, the procedure tries to maximise the the mode at the wavelength with the highest absolute number of count.

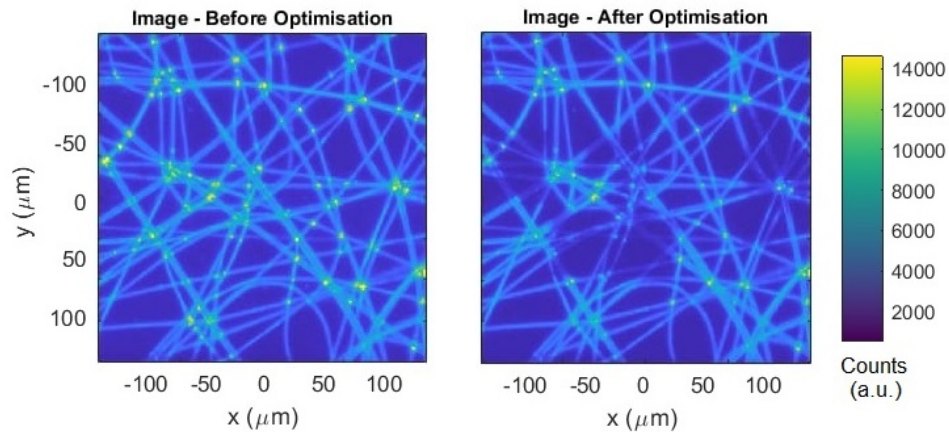


FIGURE 5.8: Image of the old sample with full illumination and optimizing pattern illumination. The counts refer to the integration over the spectrum. Lasing activity is present in both cases, as it can be seen from the peaks in number of counts at the nodes, where the laser light is scattered out. However, counts are lower in the areas that are not illuminated.

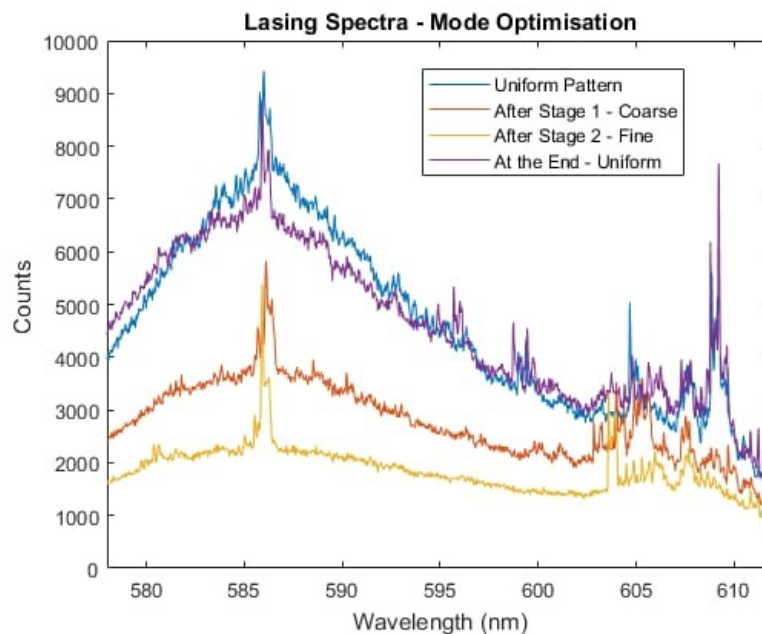


FIGURE 5.9: Lasing spectra of the old sample at full pumping power before, during, and after optimization procedure. The procedure tries to optimize the mode lasing at the wavelength with the highest number of counts when pumping the whole network. After optimization the absolute intensity of the peak is reduced, but many other modes are suppressed.

Lasing is checked on other areas of the old sample with a lower density of links. An image displaying a typical area of this kind and the illumination area is shown in figure 5.10. One of the L-L curves for a specific wavelength output

is shown in figure 5.11. It can be noticed that the output increases much more after a certain power threshold, suggesting the presence of lasing activity in the sample: this is even more clear from the spectrum plots (see figure 5.12 for an example), where various narrow spikes arise while increasing the input power.

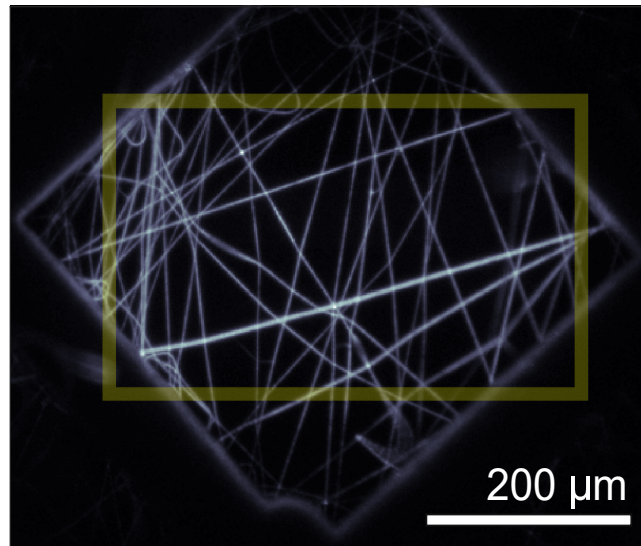


FIGURE 5.10: Image of a typical area of the old sample that has a good lasing spectrum. The yellow rectangle shows the pumping illumination area on the sample.

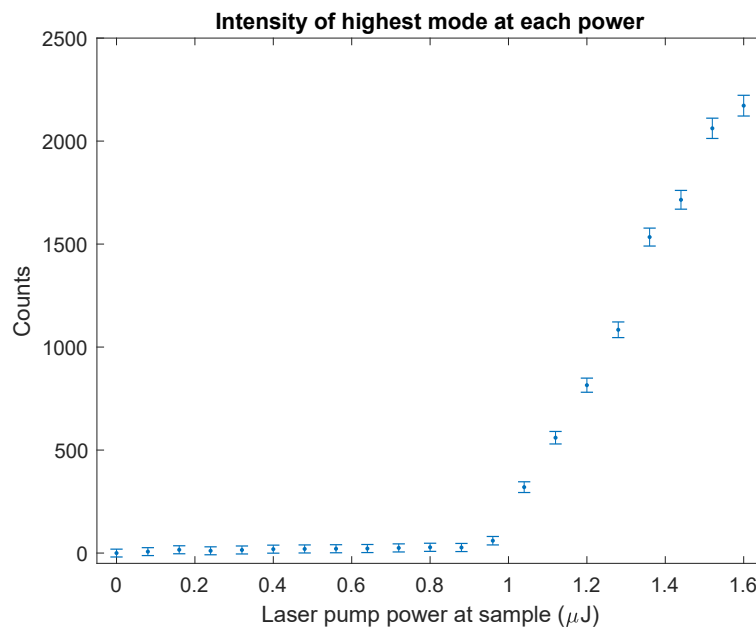


FIGURE 5.11: L-L curve for a specific wavelength in an area in the sample. The increase after a certain threshold power is a strong suggestion of lasing.

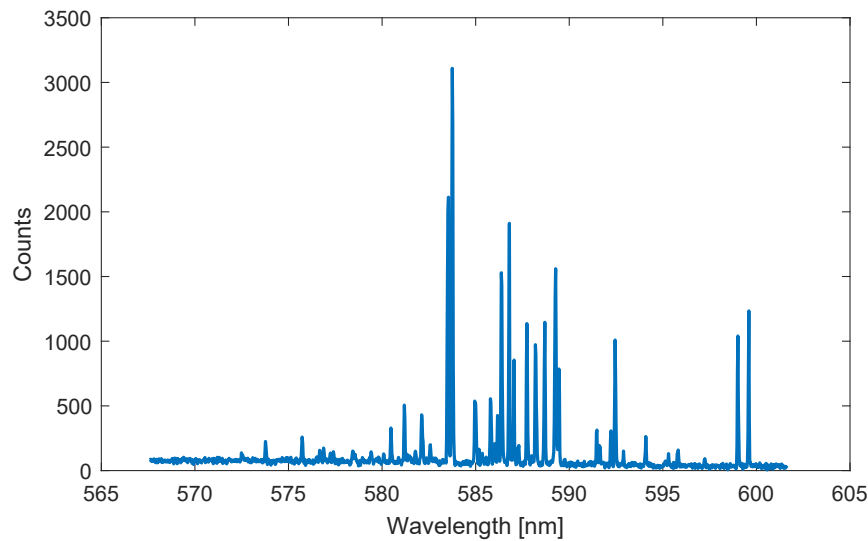


FIGURE 5.12: A typical output spectrum. The presence of many very narrow peaks that are present above certain thresholds, different for each peak, is a strong suggestion of coherent lasing.

Such areas are good candidates for the mode selections routine, since they exhibit many lasing peaks that are easily distinguishable. However, not any area is suitable, as explained in the next part.

The typical width of a lasing peak is around $\text{FWHM} \simeq 0.1 \text{ nm}$. The statistical error of a peak can be computed assuming a poissonian probability distribution for the number of counts and assuming that the peak height depends linearly on the small fluctuations of the pumping energy measured by the energy meter, that can compute RMS and PTP stability.

5.2.2 Evidence of non-linear behaviour

The non-linearity of the system is a feature that can be deduced from the results shown in section 5.2.4: in the spectra every individual peak reacts in a different manner to the switching of an area, with some decreasing in number of counts more prominently than other. This consequence of mode competition is shown in a clearer way in figure 5.13: in this case the found pattern is able to suppress many peaks, as well as increasing the height of the selected peak by a factor $\times 2$. Such effect is usually present in all areas of the sample, but it is usually seen just in few peaks during some moves, therefore is rarely seen for the selected peak.

An experiment to test the non-linearity of the system is here presented. An area of the sample is illuminated by a strip of thickness $l_{\text{thickness}}$ (measured in pixels, given that the DMD is divided in 912×1140 rectangular mirrors, the images that can be used as pattern must have sides of size 912×570 pixels, as explained in section 5.1.2) on the left side of the area and the resulting spectrum is taken. This is repeated illuminating with the same strip on the right side of the area, symmetrically. Then, the spectrum with both illumination strips is taken and compared with the sum of the two spectra taken with a

single strip of illumination. In this experiment the thickness of the strip is taken constant, $l_{\text{thickness}} = 200$ pixels, but the distance between stripes d is varied from 0 to 512 pixels. An example of the patterns used is presented in figure 5.14. The spectra taken for $d = 0$ pixels are shown in figure 5.15. The spectrum taken illuminating with both stripes has various differences with the sum of the spectra taken with just one strip of illumination: more peaks are present, some have much higher or lower number of counts than expected, while some expected peaks are not present at all (*e.g.* at around 582 nm and 588 nm two expected peaks are not measured, with the former one expected to be one of the highest modes). The difference between the measured and the expected spectra is computed for various values of strips distance d and shown in figure 5.16. Values above 0 represent peaks that were not expected or increases in expected peaks from the expected value; values below 0 represent expected peaks that are not present or decrease in expected peaks from the expected value. As anticipated, the difference is higher for strips that are closer than strips that are far apart.

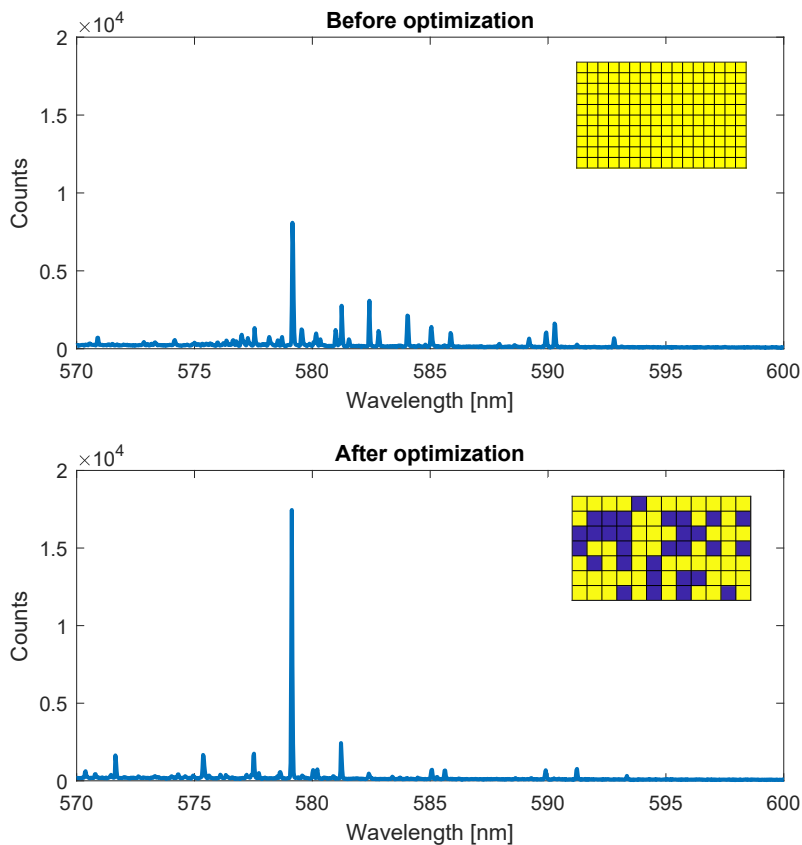


FIGURE 5.13: Spectra before and after optimization procedure. In this case, although less energy arrives at the sample, the selected mode has a higher count output after the optimization.

Such effect is a proof of the non-linearity of the system.



FIGURE 5.14: Example of patterns used: single strips of 200 pixels are first used by their own and then used together. The distance between the two strips is the parameter that is varied. In this example the distance between the strips is equal to 200 pixels.

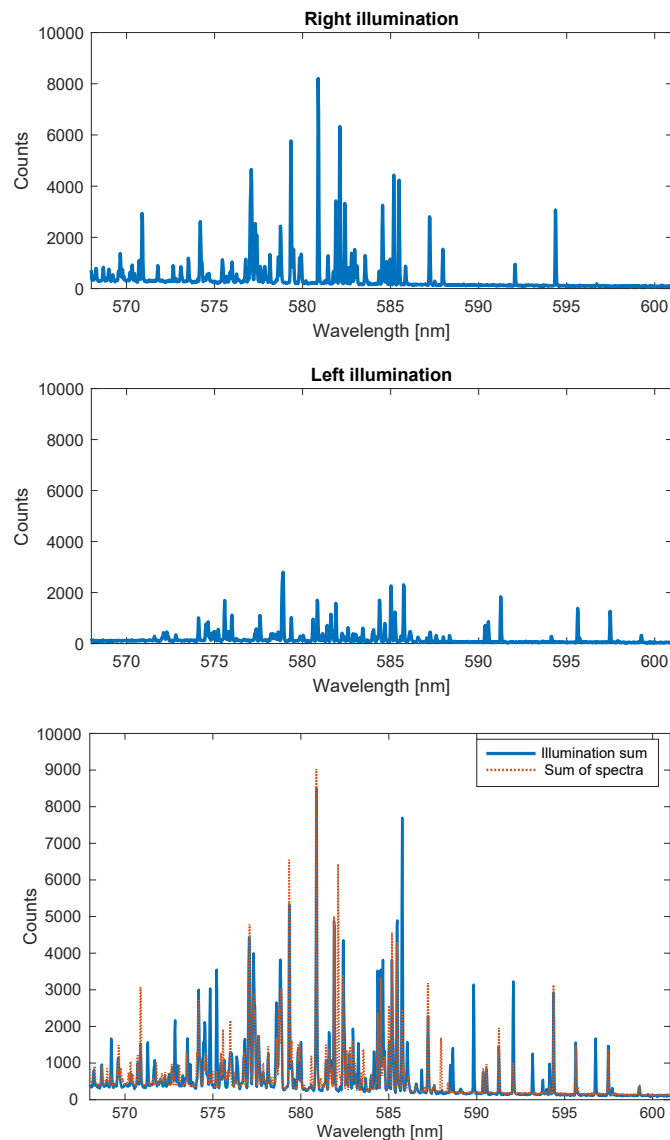


FIGURE 5.15: Spectra taken illuminating the area with a single strip (right and left). If the system reacted in a linear manner, the sum of the two outputs would have been compatible with the spectrum taken illuminating the sample with both strips. In this case, the distance between the two strips is 0 pixels.

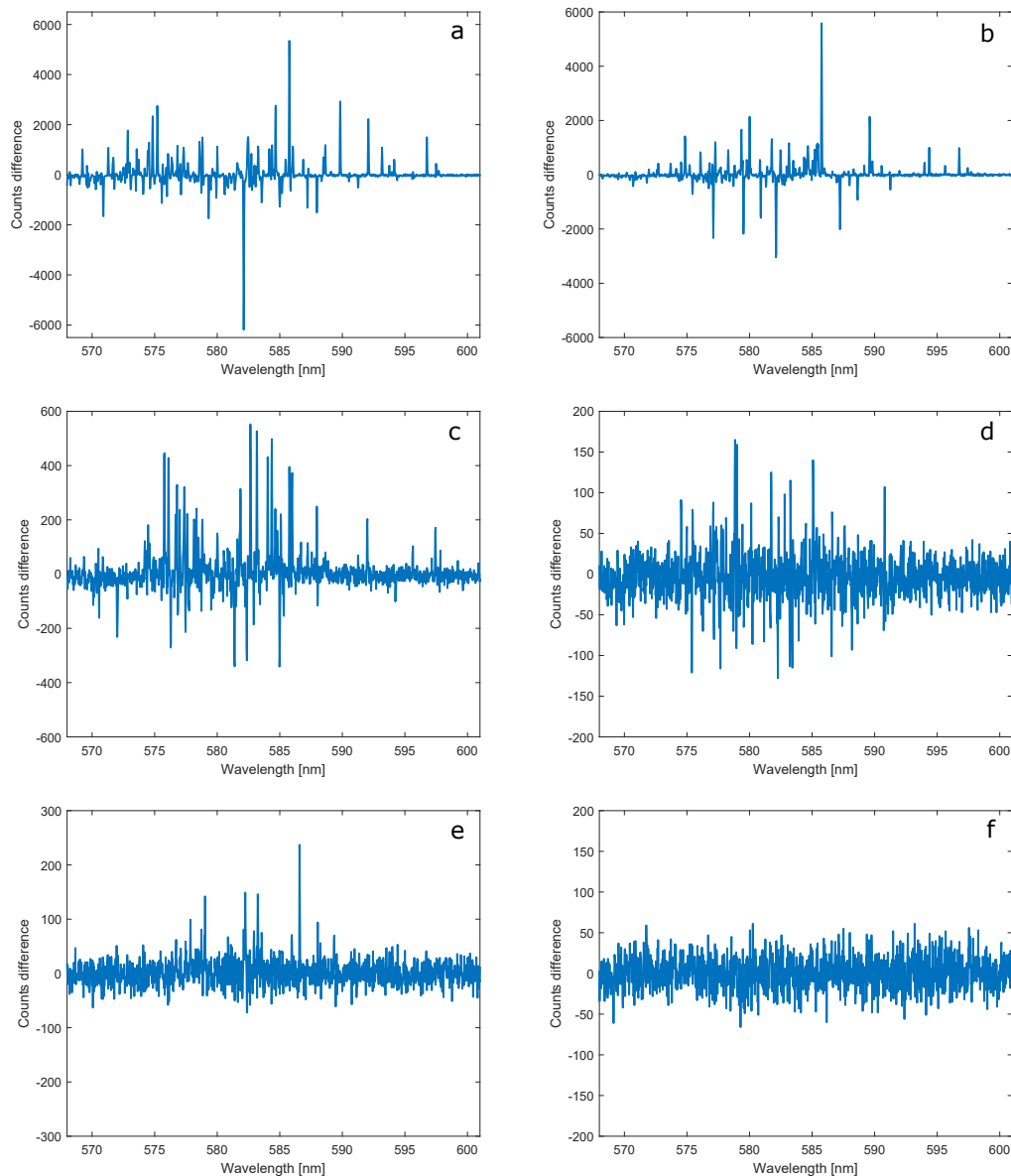


FIGURE 5.16: The difference between the spectrum taken while illuminating the sample with both strips and the sum of the two spectra taken illuminating the sample with just one strip is shown for different strip distances. Closer strips have higher non-linear effects. Distances (in pixels): a) 0, b) 52, c) 100, d) 200, e) 312, f) 512.

5.2.3 Issues with spectrum outputs

Some issues may arise while studying a certain area. One of the main issues is the spectrum shift, that, however, is easily manageable, as explained in section 5.1.3. An example of such shift can be seen in figure 5.17: the two spectra have been taken at the beginning and at the end of an optimization procedure of 160 moves. It can be noticed that after the optimization procedure the number of counts is shifted towards shorter wavelengths (the shift is around 0.025 nm

in the case in figure 5.17). Such phenomenon is still not clearly understood, some possible explanations are: it could be due to some dye property related to photobleaching; an increase in temperature of the sample that resulted in either changing the dye properties or in shrinking the PMMA waveguides; a shift in the input laser wavelength. Further investigation is therefore needed: trying to evaluate whether the shift is wavelength dependent would be a necessary first check. However, at the current situation, this effect is easily solvable and its understanding has a lower priority than other issues.

A more serious problem is stability of the area. In some areas the spectrum can change in number and intensity of peaks after few optimization procedures. Such phenomenon, that has as main cause the photobleaching of the sample, becomes more important when the area has been pumped multiple times: before the decrease in counts, photobleaching changes the gain in the various parts of the system, changing its properties. An example of this phenomenon can be seen in figure 5.18, where spectra taken from the same area, but after various illuminations, show that the spectrum has changed. Usually such effect is small in a single optimization procedure, therefore does not represent a problem if a single optimization is desired. However, such effect becomes important if multiple optimization procedures are carried out in the same area, since the first optimizations may not be valid anymore. Moreover, the exact output from the same area cannot be guaranteed also if the experiment is carried out in two different days, since the system might need to be realigned.

The presence of cosmic rays is often revealed by the spectrometer as tall peaks that appear in a measurement and disappear in the next one. They are easily recognizable by this feature, and by the narrower shape of the signal. However, it is more difficult to take them into account during the optimization procedure and may be the cause of mistakes in the optimization procedure.

The program does not take into account the presence of fluctuations: this means that some moves that were not going to affect the spectrum in a sensible way may be accepted. We may call this a "false positive". However, after one of these moves has been accepted, the probability that one more move of this kind is accepted is less likely, as the threshold for the optimization parameter has been updated to a higher value. Moreover, since these fluctuations are small, it is unlikely that the increase in threshold would be the cause of a "false negative" – a move that should have been accepted but has not been accepted due to the higher threshold. Fluctuations are also the reason why if a routine is repeated in the same area the resulting pattern is often different.

Although the optimization procedure takes into account the background, that is acquired at the beginning of each iteration, it is not able to fit an underlying incoherent fluorescence spectrum and subtract it to the measured spectrum in real-time. Therefore, the program can only use the absolute values of counts, not the relative number of counts with respect to the incoherent background.

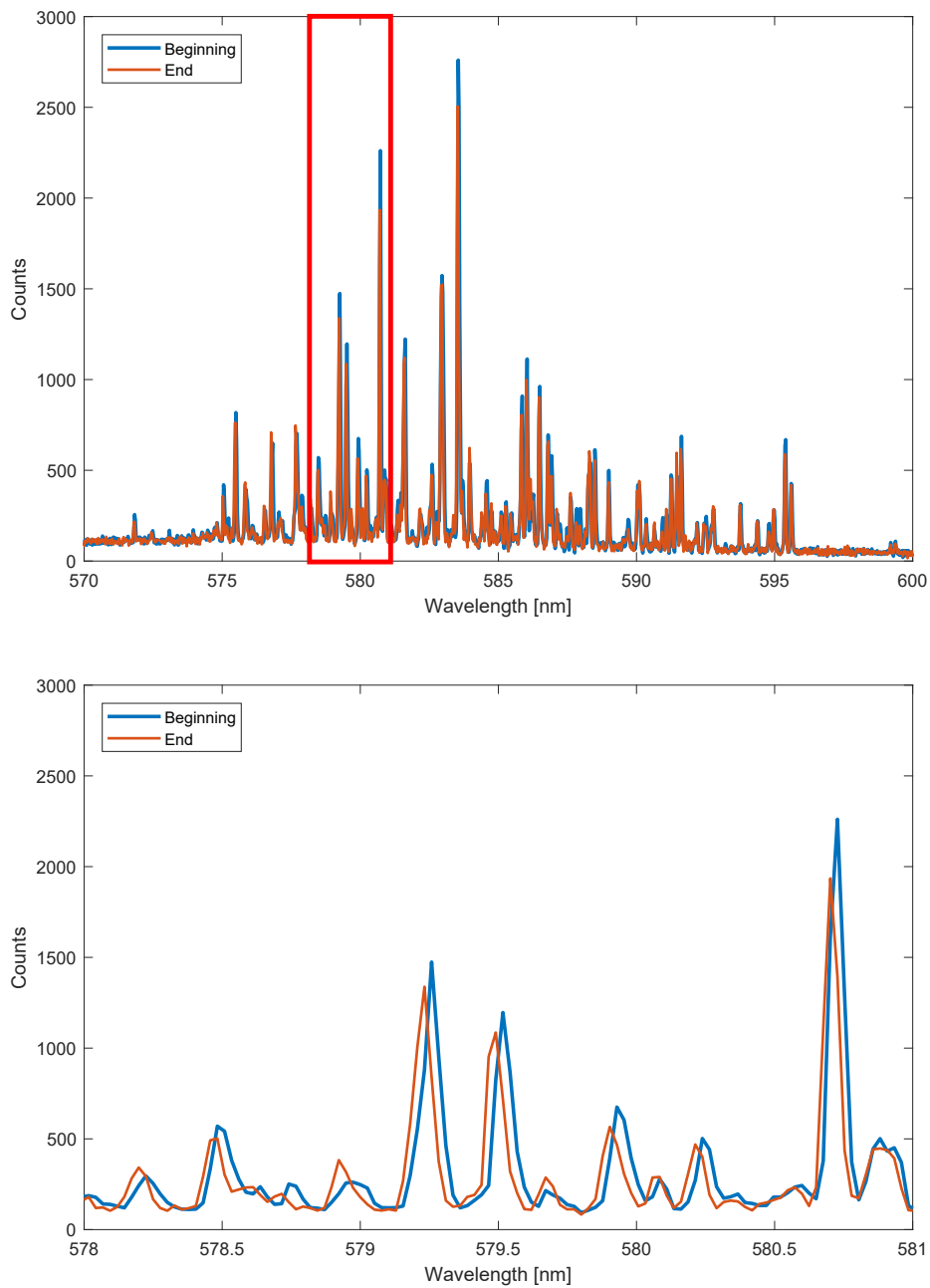


FIGURE 5.17: Example of spectrum shifting. The two spectra have been taken at the beginning and at the end of an optimization procedure of 160 moves. The highlighted region is zoomed in the second plot, where it can be noticed that after the optimization procedure the number of counts is shifted towards shorter wavelengths. The shift is around 0.025 nm.

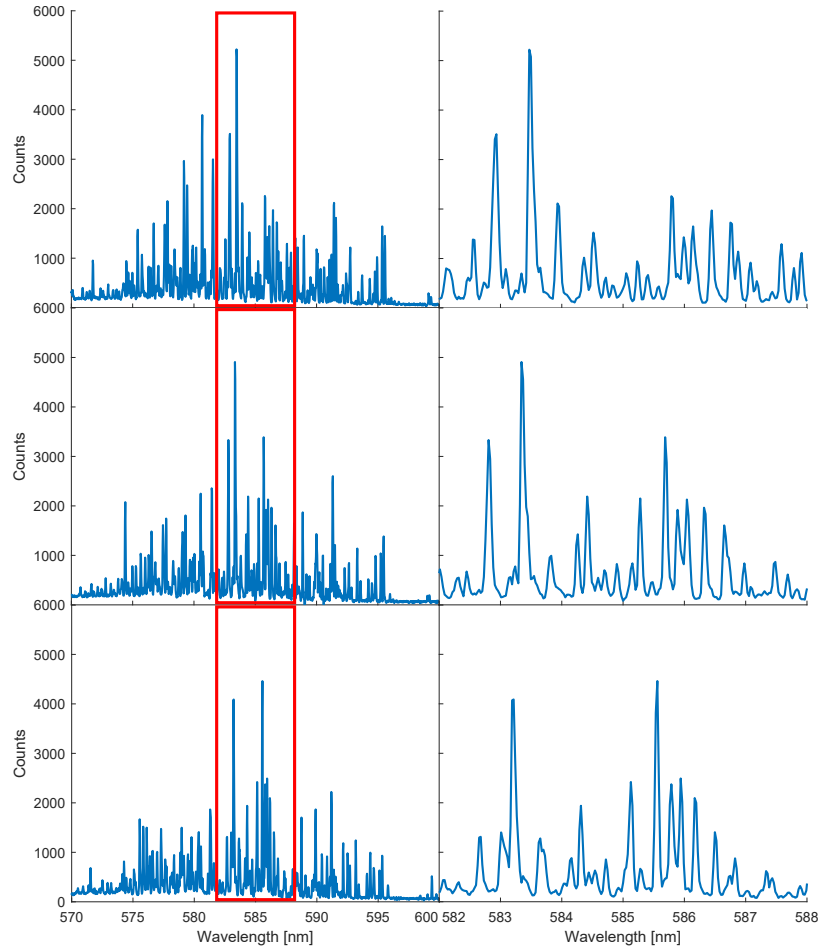


FIGURE 5.18: Example of spectral change after few optimization procedures. Spectra of the same area taken with about 10 optimization procedures between each other (that is around 1000 optimization moves). The highlighted regions are zoomed in the right plots.

5.2.4 Mode controlling

In the previous section, suitable areas in the only lasing sample have been identified. Therefore, the mode selection code is run on different parts of the sample, in order to show mode controlling by adaptive pumping. Then, limitations of the routine and of the system will be inspected. The results are here presented.

Firstly, the correct behaviour of the mode selection routine is checked experimentally. Mode suppression of all other modes but the selected one is seen during a single iteration of the routine, as in figure 5.19. In this case, the optimization parameter started from $\xi_{\text{opt,in}} = 2.92 \pm 0.04$ and reached $\xi_{\text{opt,fin}} = 7.17 \pm 0.08$ with the found optimization pattern. Good results can be obtained with a division of the field of illumination in a number of squares between 8×5 and 16×10 ; usually these two couples of values are used since the DMD is divided in 912×570 effective square pixels (see section 5.1.2 and those couples can be obtained, respectively, by dividing the DMD in squares

of size 114×114 pixels or 57×57 pixels. Moreover, coarser divisions usually are not very effective at optimizing peaks; finer divisions take up too much time, leading to unwanted bleaching-related effects, and are more susceptible to fluctuations in the spectra.

Good results can be obtained with a single iteration of the optimization routine only in a limited number of cases. In order to visit more configurations, the optimization routine can be repeated, but starting from a precedently found pattern: in this case, squares that have already been switched off will remain in such state and only squares that were switched on will be tested. The optimization can also be repeated with a finer division of the illumination area: in such case, only a multiple of the previously used division can be accepted, so that the previous final pattern can be mapped in the new divided area. The effectiveness of this method is shown in figure 5.20: the first iteration is able to suppress many modes, however many more remain; by repeating the procedure starting from the found pattern and with a finer grid it is possible to arrive to a configuration that suppresses many more modes. It is common for the selected peak to decrease in number of counts, however gaining in relative height with respect to the other modes. In the last plot, the result of another iteration of the routine starting from the previously found pattern is carried out and as a result an almost single-mode laser is achieved. The optimization parameter in the various steps of the procedure is shown in table 5.1.

Step	$\bar{\zeta}_{\text{opt}}$
Start (all-ON)	2.25 ± 0.03
8×5 pattern	3.34 ± 0.08
First 16×10 pattern	6.7 ± 0.2
Second 16×10 pattern	11.8 ± 0.6

TABLE 5.1: Optimization parameter for the spectra obtained in the various steps of the optimization procedure carried out restarting the routine from a previously found pattern shown in figure 5.20.

Restarting the routine from a previous pattern can be an effective technique for optimizing a mode, however it comes at the cost of an greater number of illuminations, increasing the likelihood of bleaching-related effects in the studied area. In order to avoid such effects, the following procedure can be carried out: instead of optimizing directly at full input energy, the optimization routine (including the possible restarts) will be carried at a lower input energy, that must, however, be above the lasing threshold of most modes; then, the energy will be increased and the routine will start from the configuration found at lower energies; this procedure can be repeated many times until reaching the desired input energy. An example of the results of this strategy can be seen in the experimental plots in figure 5.21. The top plot shows the spectrum before and after the optimization procedure, carried out with the method employed in figure 5.20, but with an input laser energy equal to 50%

of the maximum energy available. Then, the routine is repeated starting from the previously found pattern, but with an input laser energy of 75% of the maximum available energy. Since the previously found pattern has been found at a lower energy, more peaks than the selected one are now present: each optimization pattern is valid only at the energy used to find it. However, the spectrum has many less peaks compared to the all-ON configuration, therefore it is a better starting point for the optimization process. This routine is repeated again increasing the input laser energy to the maximum. Since most of the illuminations have happened at lower energies, bleaching-related issues are less likely to happen. The optimization parameter in the various steps of the procedure is shown in table 5.2.

Power	$\xi_{\text{opt,in}}$	$\xi_{\text{opt,fin}}$
50%	2.25 ± 0.03	11.8 ± 0.6
75%	3.95 ± 0.09	12.0 ± 0.6
100%	3.89 ± 0.08	9.42 ± 0.5

TABLE 5.2: Optimization parameter for the spectra obtained in the various steps of the optimization procedure carried out restarting the routine from a previously found pattern at lower pump energy shown in figure 5.21.

The mode optimization procedure proved to be successful in selecting a pattern of illumination that selects a single mode. However, in the previous figures the peak that was selected to be optimized has always been the highest one when the sample is fully illuminated and only that one. Therefore a question may arise: is the brightest mode the only mode that can be selected? This question can be broken down into two other questions: is it possible to optimize for peaks that are not the one with the highest intensity? And is it possible to optimize for different peaks in the same area? The answers are affirmative, as shown in figure 5.22. In this case, starting from the same area, two different patterns that optimize for two different peaks are found. Such peaks, that started being much weaker than the most intense ones, using the appropriate pattern become the highest peak in the spectrum. The patterns do not illuminate the central part in both cases: this could be due to the fact that most intense modes usually are found in the middle of the network. Results like these are common and achievable in many cases; however, it is not uncommon that the mode selection routine fails at optimizing for a peak, and this is found to be more likely for weaker peaks. The optimization parameter in the various steps of the procedure is shown in table 5.3.

Optimized wavelength	$\xi_{\text{opt,in}}$	$\xi_{\text{opt,fin}}$
577.0 nm	0.45 ± 0.01	3.45 ± 0.08
588.7 nm	0.73 ± 0.01	7.3 ± 0.3

TABLE 5.3: Optimization parameter for the spectra obtained optimizing for two different peaks shown in figure 5.22.

After being able to optimize different modes in the same area, the next step is to try to optimize multiple peaks at the same time. The results are presented in figure 5.23. A pattern that is able to suppress most modes apart from the two selected peaks is found and shown in the second plot from the top. In order to show that the optimization for two modes worked genuinely, it is necessary to show that it is possible to select each mode individually. This is due to the fact that the two modes might have been very correlated and that the simultaneous double optimization was achieved only because the two modes cannot be selected by their own, but only as a couple. The single mode selection procedure was carried out for each mode and the results are shown in the two bottom plot in figure 5.23. The mode at lower wavelength has been selected very nicely, as it is much higher than the very few and weak remaining modes; the other mode has been suppressed entirely. The mode at the higher wavelength has been selected, however not as nicely as the other one. Nevertheless, the selected mode is the highest mode now, few peaks are now present, and the other mode has been reduced by a much greater amount than the case of simultaneous double optimization. The optimization parameter in the various steps of the procedure is shown in table 5.4.

Optimized wavelength	$\zeta_{\text{opt,in}}$	$\zeta_{\text{opt,fin}}$
579.4 nm + 580.9 nm	1.72 ± 0.02	7.1 ± 0.2
579.4 nm	1.77 ± 0.02	4.3 ± 0.1
580.9 nm	1.37 ± 0.02	7.9 ± 0.3

TABLE 5.4: Optimization parameter for the spectra obtained optimizing for two different peaks simultaneously and then singularly shown in figure 5.23.

The last issue is about the stability of the solutions and their repeatability. Such problem may be summarized using the following question: is it possible to shine the sample with different patterns and obtain the expected output spectrum each time? Due to bleaching-related effects and wavelength blueshifting characteristics of the system we are going to consider a number of repetitions that is low enough to make those effects negligible. The last two patterns found in figure 5.23 have been used in the same area for this analysis. Those two patterns have been used in alternation to shine the sample for ten times each. In figure 5.24 the spectrum of each illumination is represented as a heatmap: each horizontal strip represent the spectrum of a single illumination, while the number of counts is represented with colours. The alternation between different patterns is visible from the alternation of the same two spectra: however, a more rigorous calculation is needed to assess the degree of compatibility of the spectra. In order to compute the compatibility parameter between two spectra the following procedure has been carried out: the compatibility between number of counts for each bin has been calculated; then, only the bins with a count number greater than 300 have been considered, in order to avoid having as main contributor to the parameter the fluorescence baseline; the average compatibility has been used

as compatibility between spectra. The compatibility parameter c between bins has been calculated using the following formula:

$$c = \frac{|h_1 - h_2|}{\sqrt{\sigma_1^2 + \sigma_2^2}}, \quad (5.2)$$

where h_i is the number of counts in measurement i and σ_i is its standard deviation. Lower values are representative of more compatible measures. The compatibility with the first spectrum and the compatibility with the average spectrum have been calculated for both patterns. The compatibilities between spectra are computed and shown in figure 5.25. Most spectra are highly compatible between each other; moreover, looking at the plots about the compatibility with the first spectrum, no clear increase in compatibility parameter (*i.e.* decrease in compatibility) is present at higher repetition numbers.

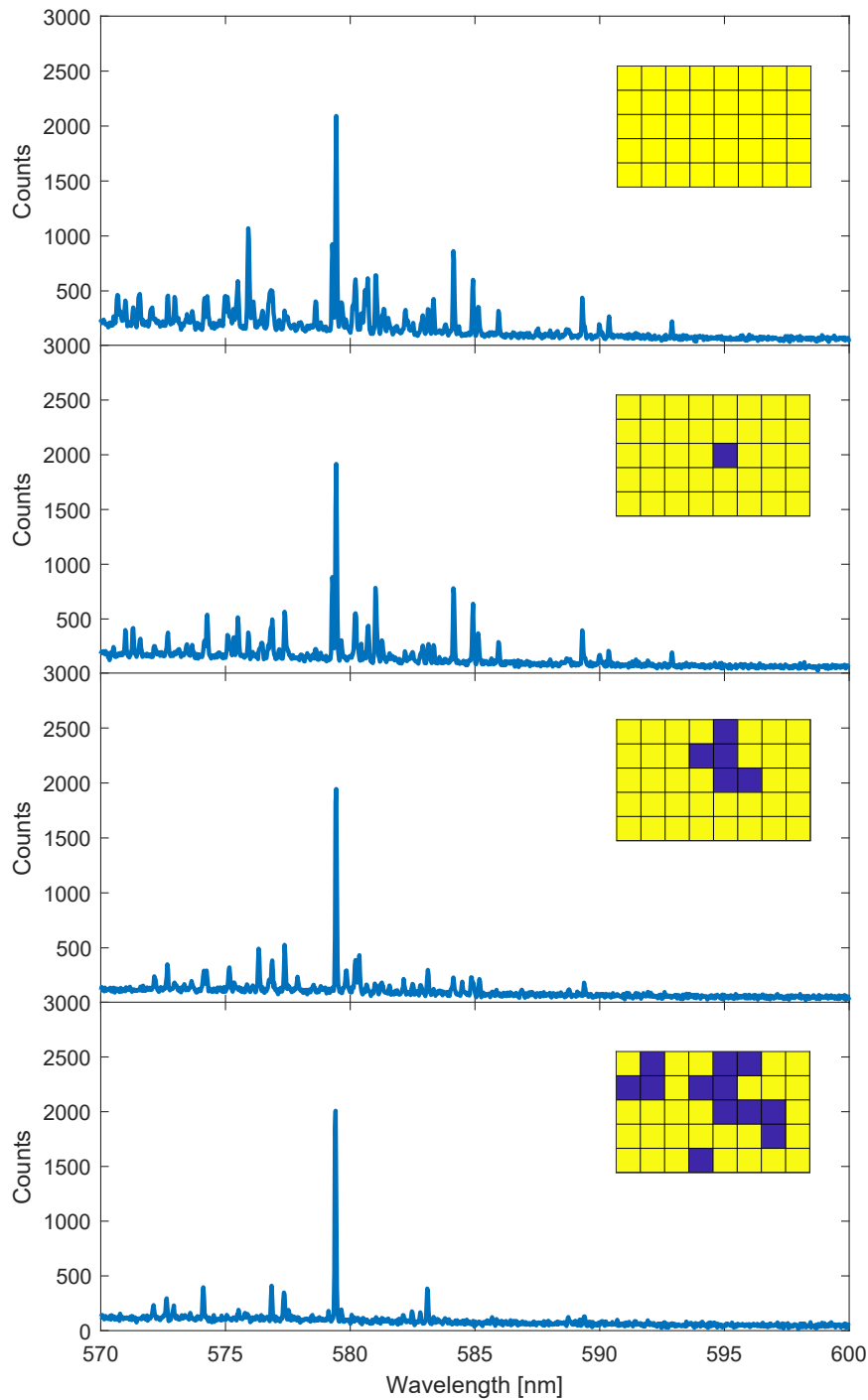


FIGURE 5.19: Some spectra during the optimization procedure are shown with the relative pattern. Peaks that have not been selected decrease while the routine proceeds. The corresponding patterns are shown as insets: yellow is used for shined areas, while blue is used for areas that have not been illuminated.

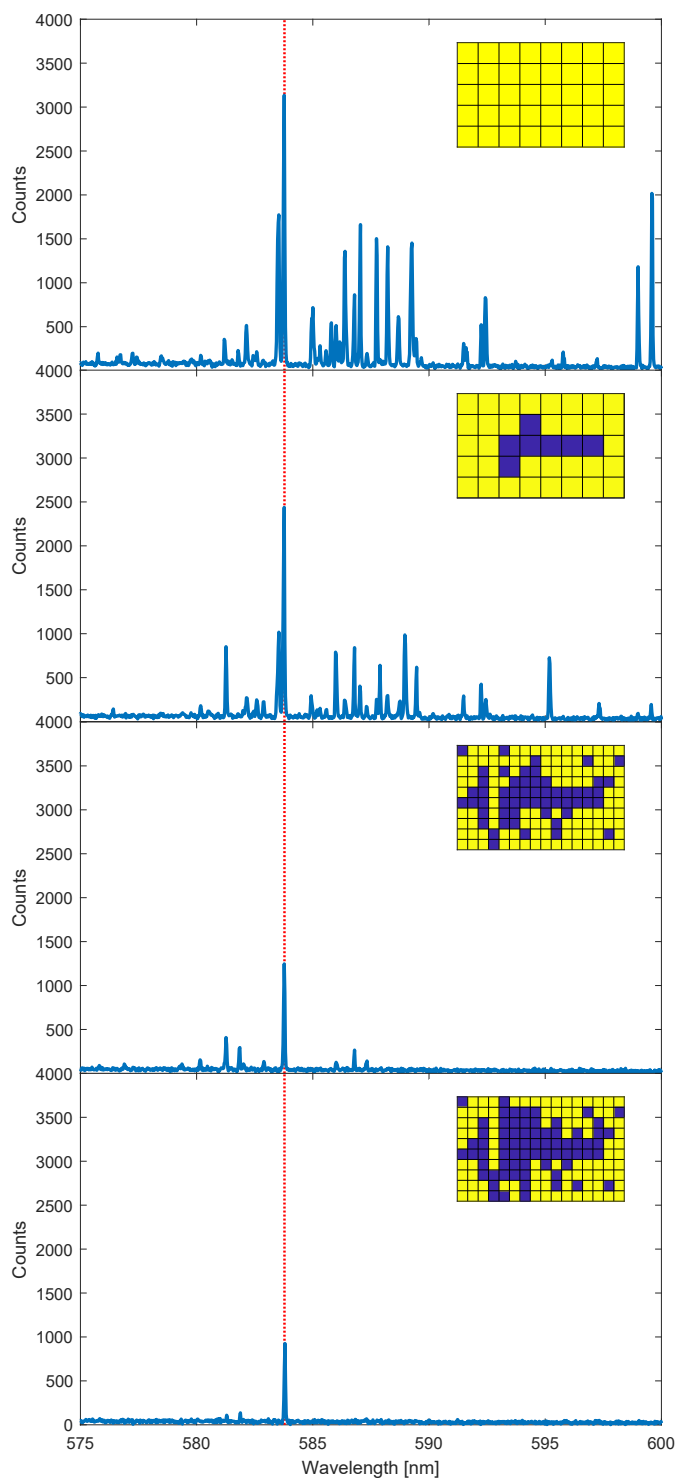


FIGURE 5.20: Optimization procedure for the wavelength marked with the red dashed line carried out restarting the routine from the configuration previously found. A finer grid is used after the second plot, as shown in the inlets representing the used patterns (yellow = ON, blue = OFF).

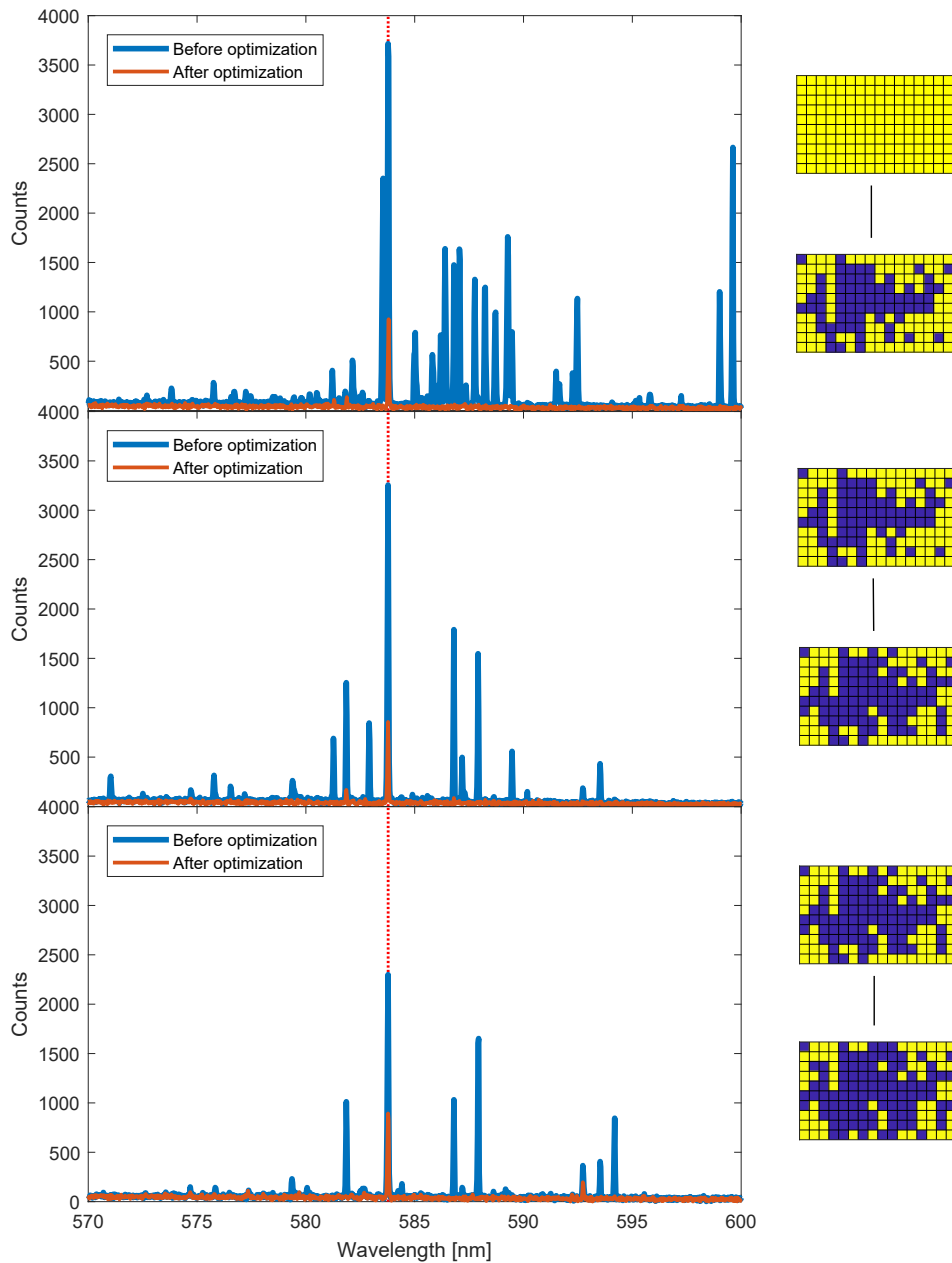


FIGURE 5.21: Optimization procedure carried out at different energies and restarting from the configurations found using a lower energies. In this case, the used energy fractions are 50% for the top plot, 75% for the middle plot, and 100% for the bottom plot. The starting and final patterns are shown beside the plots (yellow = ON, blue = OFF).

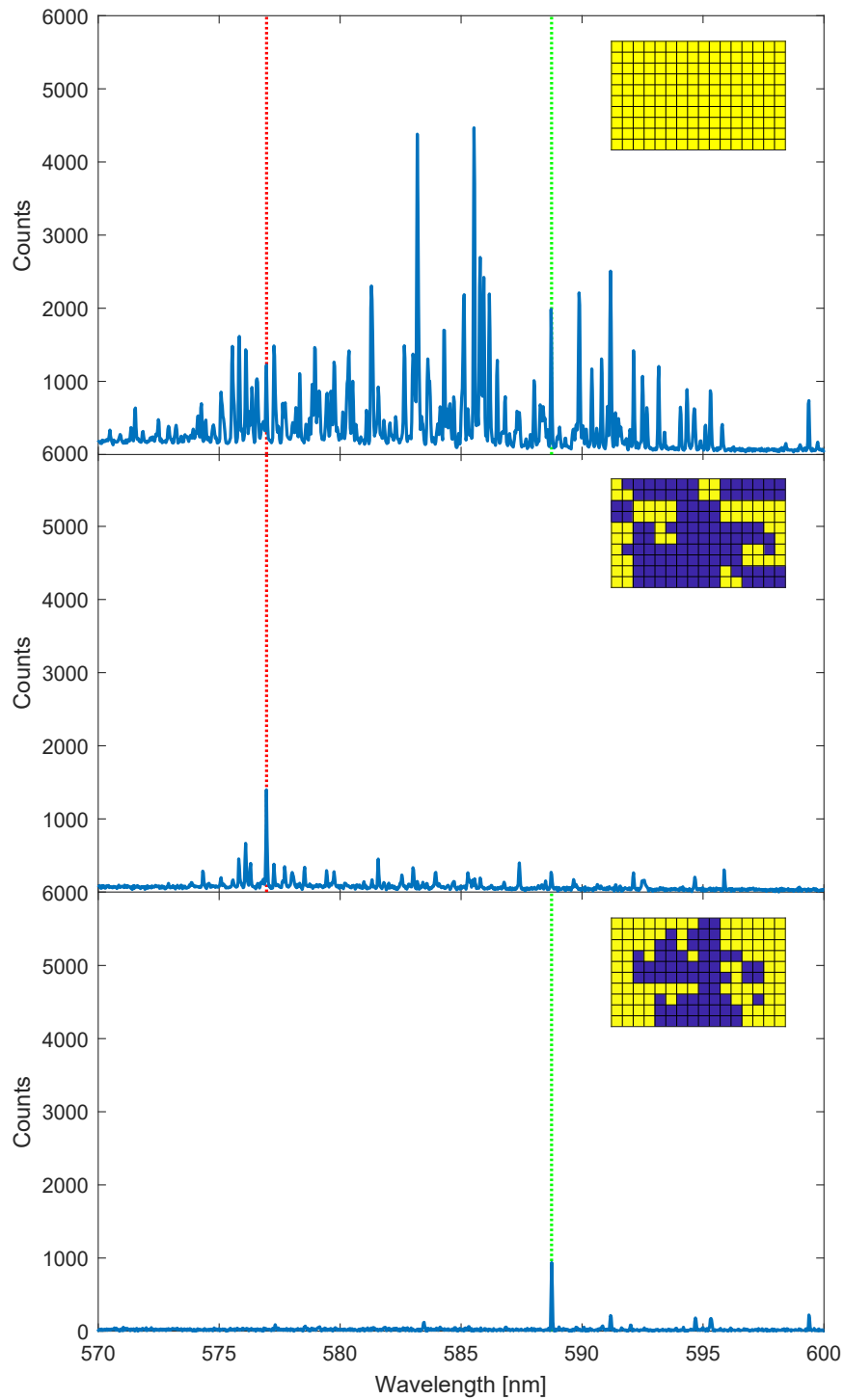


FIGURE 5.22: The optimization procedure has been carried out for two different peaks (marked with two dashed vertical lines), with two distant wavelengths, starting from the same initial spectrum (top). The used patterns are shown inside the inlets (yellow = ON, blue = OFF).

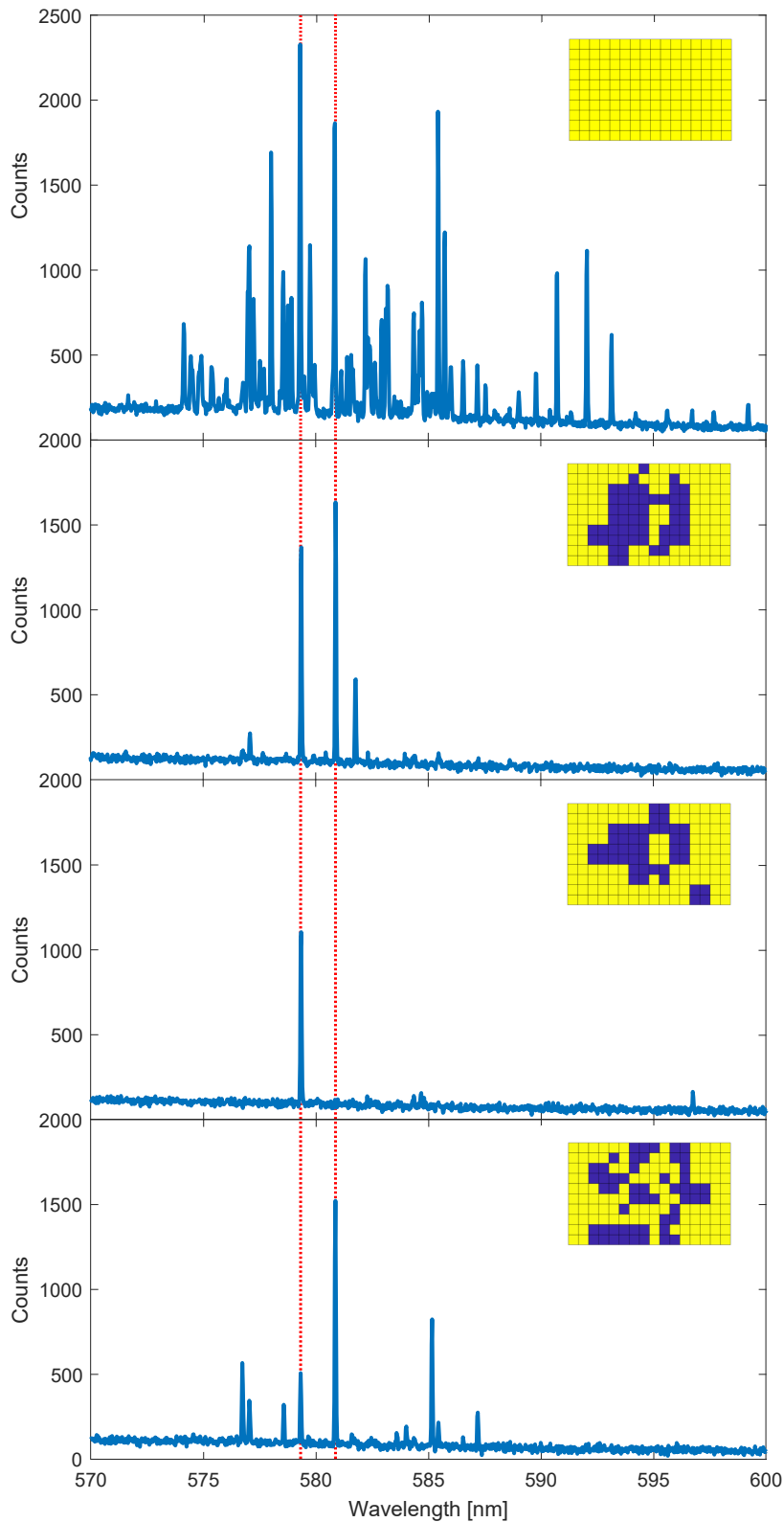


FIGURE 5.23: The optimization procedure has been carried out starting from the initial spectrum (top) trying to optimize two different peaks at the same time (second plot). The procedure has then been repeated for each mode singularly. The used patterns are shown inside the inlets (yellow = ON, blue = OFF).

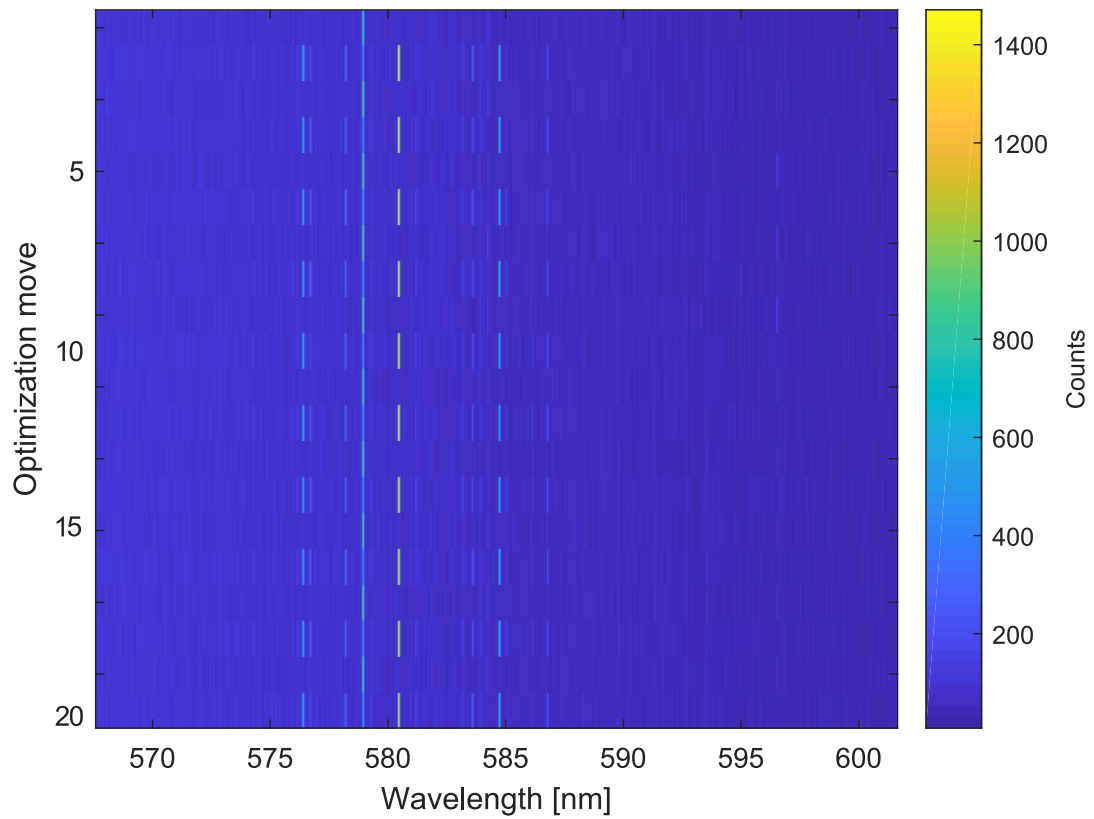


FIGURE 5.24: Two patterns, found by optimizing for two different wavelengths in the same area, are used to illuminate that area in alternation. It can be seen that each pattern selects the desired peak at every iteration.

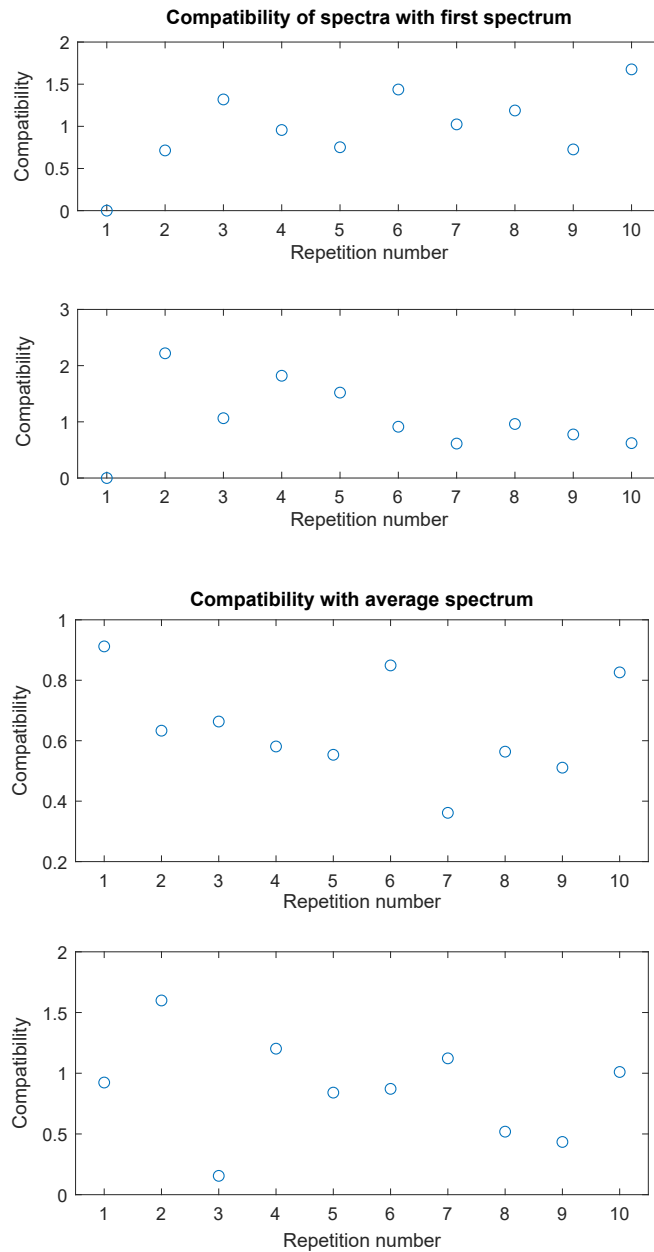


FIGURE 5.25: The compatibility between spectra of the same pattern are calculated. The compatibility with the first spectrum shows that the output is relatively stable in time, otherwise would increase in time.

Chapter 6

Concluding chapter

6.1 Future developments

Some of the possible next steps include: identifying a strategy to select a mode with few steps using a big number of networks and applying a machine learning algorithm; studying different network topologies and defining parameters to quantify the controllability of networks and modes; using different types of network samples that are less prone to photobleaching effects. Changing the setup in order to manipulate the refractive index of single links or to measure the directionality of the laser light produced by the network are some of the directions that can be taken in the future.

6.2 Conclusions

In this work, mode selection in a network random laser through a reliable procedure has been demonstrated. A computational approach to the problem has been carried out by creating a program that simulates the experimental mode selection routine, by calculating the loss of each mode and the gain that they receive when some links are pumped. Preliminary studies are carried out on Buffon-type networks and show that particular link ordering and functions \mathcal{G} are more convenient than others in terms of speed and accuracy. The experimental mode selection procedure in a network random laser has been built accordingly and has proved to be an effective procedure to select a mode, given that the chosen area allows it. Multiple versions of the procedure have been used, trying to minimize the unwanted photobleaching-related effects. The procedure allows to select different modes arising in the same area and optimize them either individually or in groups.

Bibliography

- [1] Barabasi, A. "The network takeover." *Nature Physics* 8 (2011)
- [2] Z. Q. Zhang, C. C. Wong, K. K. Fung, Y. L. Ho, W. L. Chan, S. C. Kan, T. L. Chan, and N. Cheung, *Physical Review Letters* 81 (1998).
- [3] H. Cao, *J. Phys. A: Math. Gen.* 38 (2005)
- [4] Gaio, M., Saxena, D. et al. "A nanophotonic laser on a graph." *Nature Communications* 10, 226 (2019)
- [5] Gould, R. Gordon "The LASER, Light Amplification by Stimulated Emission of Radiation". *The Ann Arbor Conference on Optical Pumping, the University of Michigan, 15 June through 18 June 1959* (1959)
- [6] V. S. Letokhov, "Generation of light by a scattering medium with negative resonance absorption" *Soviet Physics JETP* (1968)
- [7] R. Balachandran and N. Lawandy, "Laser action in strongly scattering media," *Nature* 368 (1994)
- [8] H. Cao et al. "Random Laser Action in Semiconductor Powder" *Physical Review Letters* 28 (1999)
- [9] S. V. Florov et al. "Laser-like emission in opal photonic crystals" *Optics Communications*, 162(4) (1999)
- [10] S. Mujumdar et al. "Amplified Extended Modes in Random Lasers" *Physical Review Letters* 93, 053903 (2004)
- [11] V. M. Apalkov, M. E. Raikh, and B. Shapiro "Anomalous Localized States in the Anderson Model" *Phys. Rev. Lett.* 92 (2004)
- [12] L. Ge, Y. D. Chong, A. D. Stones "Steady-state Ab Initio Laser Theory: Generalizations and Analytic Results" *Physical Review A* 82(6) (2010)
- [13] X. Jiang, C. M. Soukoulis "Theory and Simulations of Random Lasers" *Photonic Crystals and Light Localization in the 21st Century* pp 417-433 (2000)
- [14] C. Vanneste and P. Sebbah, "Selective Excitation of Localized Modes in Active Random Media," *Phys. Rev. Lett.* 87 (2001)
- [15] P. W. Anderson, *Phys. Rev.* 109 (1958)
- [16] A. F. Ioffe, A. R. Regel, *Prog. Semicond.* 4 (1960)

- [17] J. Liu, P. D. Garcia, S. Ek, N. Gregersen, T. Suhr, M. Schubert, J. Mørk, S. Stobbe, and P. Lodahl, *Nat Nano* 9 (2014)
- [18] M. Gaio, M. Moffa, M. Castro-Lopez, D. Pisignano, A. Camposeo, and R. Sapienza, *ACS Nano* 10 (2016).
- [19] D. S. Wiersma, *Nat. Phys.* 4, 359 (2008)
- [20] Bachelard, N., et al. "Adaptive pumping for spectral control of random lasers." *Nature Physics* 10, 426–431 (2014)
- [21] Liew, S. F., et al. "Active control of emission directionality of semiconductor microdisk lasers." *Appl. Phys. Lett.* 104, 231108 (2014)
- [22] Sznitko, L. "The role of polymers in random lasing." *Journal of Polymer Science, Part B: Polymer Physics* 53 (2015)
- [23] A. L. Barabasi "Network Science" *Cambridge University Press* (2016)
- [24] R. Albert, A. L. Barabasi "Statistical mechanics of complex networks" *Reviews of Modern Physics* 74 (2002)
- [25] Saleh, Mahmoud; Esa, Yusef; Mohamed, Ahmed "Applications of Complex Network Analysis in Electric Power Systems" *Energies* 11 (2018)
- [26] Wasserman, Stanley and Katherine Faust "Social Network Analysis: Methods and Applications" *Cambridge University Press* (1994)
- [27] A. Bashan et al " Network physiology reveals relations between network topology and physiological function" *Nature Communications* 3: 702 (2012)
- [28] Habibi, Iman; Emamian, Effat S.; Abdi, Ali "Advanced Fault Diagnosis Methods in Molecular Networks" *PLOS ONE* 9 (2014)
- [29] Friedman, J., and Tillich, J.P. "Wave equations for graphs and the edge-based Laplacian" *Journal of Mathematics*, 216 (2004)
- [30] Kuchment, P. "Quantum graphs: I. Some basic structures" *Waves Random Media* 14, S107–S128 (2004)
- [31] L. Bottcher "Extending Buffon's Needle Problem to Random-Line Graphs" (2019)
- [32] A. Camposeo et al. "Laser Emission from Electrospun Polymer Nanofibers" *Small* 5 (2009)
- [33] Yarborough, J. M. "CW dye laser emission spanning the visible spectrum" *Applied Physics Letters* 24 (1974)
- [34] L. Persano, A. Camposeo, D. Pisignano "Advancing the Science and Technology of Electrospinning and Functional Nanofibers" *Macromol. Mater. Eng.* 302 (2017)

-
- [35] M. Gaio, M. Moffa, M. Castro-Lopez, D. Pisignano, A. Camposeo, and R. Sapienza "Modal Coupling of Single Photon Emitters Within Nanofiber Waveguides" *ACS Nano* 10, 6125 (2016)